



Universidad de Valladolid



**ESCUELA DE INGENIERÍAS
INDUSTRIALES**

**UNIVERSIDAD DE VALLADOLID
ESCUELA DE INGENIERIAS INDUSTRIALES**

MÁSTER EN INGENIERÍA QUÍMICA

Recrystallization kinetics of API/polymer systems

Autor: Rodríguez del Egado, Miguel Guillermo

**Responsable Intercambio UVa:
Mato Chaín, Rafael B.**

Technische Universität Dortmund

Valladolid, Mayo 2017.

TFM REALIZADO EN PROGRAMA DE INTERCAMBIO

TÍTULO: **Recrystallization kinetics of API/polymer systems**

ALUMNO: **Miguel Guillermo Rodríguez del Egido**

FECHA: **18/04/2017**

CENTRO: **Technische Universität Dortmund**

TUTOR: **Christian Lübbert**

Palabras clave: Recristalización, compuesto farmacéutico, nifedipina, dispersión sólida, Avrami.

Resumen: El compuesto nifedipina es prácticamente insoluble en agua y consecuentemente no se alcanza todo el potencial de sus propiedades. Para superar estas limitaciones, se utiliza la técnica de dispersión sólida. Sin embargo, formulaciones en estado amorfo obtenidas tienden a recristalizar.

Se estudiaron diferentes factores influyentes en la recristalización. De acuerdo a la composición de la formulación, cuanto menor concentración del compuesto farmacéutico, mayor es el tiempo para cristalizar. Respecto a la humedad relativa (RH), existe una gran diferencia entre los valores iniciales y finales de agua absorbida en los experimentos con las RH implementadas. Respecto a la temperatura, cuanto menor es la temperatura, mayor es tiempo necesario para alcanzar el equilibrio. También se llevaron a cabo experimentos cambiando el polímero y el modo de preparar la formulación.

Para caracterizar las muestras se utilizaron Powder X-Ray Diffraction (PXRD), Differential Scanning Calorimetry (DSC) y espectrofotómetro.

La ecuación de Avrami ha demostrado su validez para modelar el comportamiento seguido por la cristalización.

Technische Universität Dortmund
Fakultät Bio- und Chemieingenieurwesen

Lehrstuhl für Thermodynamik

Recrystallization kinetics of API/polymer systems

Master-Thesis

Miguel Guillermo Rodríguez del Egado

Matriculation Number: 197306

Dortmund, 18.04.2017

Supervisor: M. Sc. Christian Lübbert
First Examiner: Prof. Dr. Gabriele Sadowski
Second Examiner: Prof. Dr. Gerhard Schembecker

Declaration of authorship

I affirm that this thesis is completely my work and that any material from other sources is marked in the text to the best of my knowledge. I also assure that I have not submitted any part of this work for a degree at any other institution.

Dortmund 18.04.2017

Miguel Guillermo Rodríguez del Egado

Abstract

The goal of this master project is to study the crystallization of nifedipine from water content absorbed by analyzing different influencing: active pharmaceutical ingredients (API) weight fraction, temperature, relative humidity (RH), polymer and the method to prepare the formulation.

The drug is practically insoluble in water, consequently its properties do not reach its full potential. To overcome these limitations, the solid dispersion method was the solution. It was originally used to improve the dissolution properties and the bioavailability of poorly water soluble drugs by dispersing them into water soluble carriers.

The amorphous solid dispersions were prepared by spray drying method with a Büchi Mini Spray Dryer B-290.

When preparing the formulation, the same steps were always followed in order to have the same thermodynamic history for all the samples. When preparing the amorphous solid dispersion, acetone was used as solvent. The inlet temperature was 60 °C and the outlet temperature was in a range of 35-40 °C.

After spray drying or melting method, the results show that the solid dispersions were totally amorphous. In order to characterize the solid state of the sample, powder X-ray diffraction (PXDR) and differential scanning calorimetry (DSC) were used.

The Avrami equation has proved its validity to model the behavior followed by the crystallization. The parameters obtained agree with the results achieved from the suspension balance experiments. It has been shown that the assumption of n parameter equal to 4, which is crystal growth in 3 dimensions, is correct.

According to the API weight fraction, the lower API concentration the sample contains, the longer it takes to crystallize. It could be the case that with that weight fraction does not reach the recommended dose, in that case it would have to reach a compromise between the weight fraction and the improved properties achieved and the recommended dose. On the other side, future investigations would go in the direction of studying lower API weight fractions.

In terms of relative humidity, a huge difference occurs among the several relative humidities that have been implemented. These differences translate into variations in the time required to reach the equilibrium and crystallize and the initial and final water content.

Regarding to the temperature, the lower temperature under the sample is at, the longer it takes to crystallize. Thereby, in order to avoid crystallization, it is necessary to operate under a minimum temperature.

In respect of the method to prepare the formulation, differences in time to crystallize emerged. Thus, the time needed for the melting method, which is normally used in industry, is less than the time required for spray drying method. In this manner, in order to avoid crystallization, it might be considered a way to use and optimize the spray drying method on a large scale.

Respecting the polymer used in the formulation, it was noticed that PVAC retarded the time to crystallize so that it better fulfills the purpose of avoiding crystallization than Resomer R203s. In further investigations, more polymers will have to be studied in order to find the optimum.

List of symbols

| Symbol | Interpretation |
|-----------|-------------------------------|
| w_{API} | Weight fraction of API |
| w_{NIF} | Weight fraction of Nifedipine |
| T_{in} | Inlet temperature |
| T_{out} | Outlet temperature |

List of abbreviations

| Abbreviation | Interpretation |
|--------------|--|
| API | Active Pharmaceutical Ingredient |
| NIF | Nifedipine |
| FDA | Food and Drug Administration |
| RH | Relative humidity |
| PXRD | Powder X-Ray Diffraction |
| DSC | Differential Scanning Calorimetry |
| UV-Vis | Ultra Violet – Visible |
| A | Absorbance |
| VLE | Vapor Liquid Equilibrium |
| SVLE | Solid Vapor Liquid Equilibrium |
| PVAC | Polyvinyl acetate of molecular weight 90.000 g/mol |
| PVAC350 | Polyvinyl acetate of molecular weight 350.000 g/mol |
| SD | Solid dispersion |

List of figures

| | |
|--|----|
| Figure 1. Scheme of spray drying method [6]..... | 5 |
| Figure 2 Hot melt extrusion process [7]..... | 7 |
| Figure 3. PXDR pattern of an amorphous sample (w_{NIF} 70%)..... | 8 |
| Figure 4. PXDR pattern of a recrystallized sample (w_{NIF} 80%, PVAC350, 40°C, 75%RH) obtained after the suspension balance experiment | 8 |
| Figure 5. DSC thermogram of NIF/PVAC (w_{NIF} 70%, PVAC, 40°C, 75%RH)..... | 9 |
| Figure 6. Behavior of solubility against temperature and API weight fraction [10] | 10 |
| Figure 7. Behavior of solubility and present phases against temperature and weight fraction [10] | 11 |
| Figure 8. Evolution of water weight fraction: (a) initial curve for amorphous formulation at temperature I, (b) at temperature II, and (c) at temperature III [10] | 11 |
| Figure 9. Behavior of NIF solubility [10]..... | 12 |
| Figure 10. Behavior of water content and phases during crystallization for a w_{NIF} 70% [10]..... | 13 |
| Figure 11. Interaction of the three components of the system..... | 16 |
| Figure 12. Interaction of the forces involved in the EoS..... | 17 |
| Figure 13. Characteristic sigmoidal curve followed by crystallization [16] | 20 |
| Figure 14. Graph where the slope is the n parameter [17] | 21 |
| Figure 15. Molecular structure of NIF | 22 |
| Figure 16. Molecular structure of NIF polymorphs [23] | 23 |
| Figure 17. Behavior of the two polymorphs on heating and cooling [23]..... | 24 |
| Figure 18. Theoretical NIF pattern by PXRD | 24 |
| Figure 19. Büchi Mini Spray Dryer B-290 experimental installation | 26 |
| Figure 20. Suspension balance experimental installation | 27 |
| Figure 21. Rigaku Miniflex 600 equipment..... | 29 |
| Figure 22. TA Instruments DSC Q-2000 equipment..... | 30 |
| Figure 23. Eppendorf BioSpectrometer equipment | 31 |
| Figure 24. Fitting of the experimental and VLE NIF curves [25]..... | 33 |
| Figure 25. Sorption diagram for sample w_{NIF} 80%, 40°C, 60°RH..... | 34 |
| Figure 26. Sorption diagram for sample w_{NIF} 80%, 40°C, 75°RH..... | 35 |
| Figure 27. Sorption diagram for sample w_{NIF} 80%, 40°C, 90°RH..... | 35 |
| Figure 28. Sorption diagram for sample w_{NIF} 80%, 35°C, 75°RH..... | 36 |
| Figure 29. Sorption diagram for sample w_{NIF} 80%, 30°C, 75°RH..... | 36 |
| Figure 30. Overlap of the two independent water sorption measurements obtained for $w_{NIF}=0.80$ at 40 °C, 75% RH to check the reproducibility of the experiments | 37 |
| Figure 31. Evolution of water content along the weight fraction..... | 38 |
| Figure 32. Evolution of water content along RH..... | 39 |
| Figure 33. Evolution of water content along temperature for w_{NIF} 90% and 75%RH..... | 40 |
| Figure 34. Evolution of water content along temperature for w_{NIF} 80% and 75%RH..... | 40 |
| Figure 35. Evolution of water content along temperature for w_{NIF} 70% and 75%RH..... | 41 |
| Figure 36. Evolution of water content along polymer for w_{NIF} 80%, 40°C and 75%RH..... | 42 |
| Figure 37. Evolution of water content along the method to prepare the formulation for w_{NIF} 80%, 40°C and 75%RH..... | 43 |
| Figure 38. Concentration of compounds in the liquid phase for reference sample (w_{NIF} 80%, 40°C, 75%RH)..... | 45 |

| | |
|--|----|
| Figure 39. Evolution of concentration of crystals, water and API for reference sample (w_{NIF} 80%, 40°C, 75%RH)..... | 45 |
| Figure 40. PXRD pattern of amorphous state of sample w_{NIF} 80%..... | 46 |
| Figure 41. PXDR pattern of crystalline state of sample w_{NIF} 80%, 40°C and 75%RH..... | 46 |
| Figure 42. Coupling of the experimental curve and Avrami theoretical curve | 49 |
| Figure 43. K coefficient behavior with API weight fraction | 50 |
| Figure 44. K coefficient behavior with relative humidity..... | 51 |
| Figure 45. K coefficient behavior as function of temperature..... | 53 |
| Figure 46. Concentration of components in the liquid phase for sample w_{NIF} 0.90, 40°C, 75%RH | 58 |
| Figure 47. Evolution of concentration of crystals, water and API for sample w_{NIF} 0.90, 40°C, 75%RH | 58 |
| Figure 48. Concentration of components in the liquid phase for sample w_{NIF} 0.70, 40°C, 75%RH | 58 |
| Figure 49. Evolution of concentration of crystals, water and API for sample w_{NIF} 0.70, 40°C, 75%RH | 59 |
| Figure 50. Concentration of components in the liquid phase for sample w_{NIF} 0.85, 40°C, 75%RH | 59 |
| Figure 51. Evolution of concentration of crystals, water and API for sample w_{NIF} 0.85, 40°C, 75%RH | 59 |
| Figure 52. Concentration of components in the liquid phase for sample w_{NIF} 0.75, 40°C, 75%RH | 60 |
| Figure 53. Evolution of concentration of crystals, water and API for sample w_{NIF} 0.75, 40°C, 75%RH | 60 |
| Figure 54. Concentration of components in the liquid phase for sample w_{NIF} 0.80, 40°C, 75%RH by melting-cooling..... | 60 |
| Figure 55. Evolution of concentration of crystals, water and API for sample w_{NIF} 0.80, 40°C, 75%RH by melting-cooling | 61 |
| Figure 56. Concentration of components in the liquid phase for sample w_{NIF} 0.80, 40°C, 90%RH | 61 |
| Figure 57. Evolution of concentration of crystals, water and API for sample w_{NIF} 0.80, 40°C, 90%RH | 61 |
| Figure 58. Concentration of components in the liquid phase for sample w_{NIF} 0.80, 40°C, 60%RH | 62 |
| Figure 59. Evolution of concentration of crystals, water and API for sample w_{NIF} 0.80, 40°C, 60%RH | 62 |
| Figure 60. Concentration of components in the liquid phase for sample w_{NIF} 0.90, 30°C, 75%RH | 62 |
| Figure 61. Evolution of concentration of crystals, water and API for sample w_{NIF} 0.90, 30°C, 75%RH | 63 |
| Figure 62. Concentration of components in the liquid phase for sample w_{NIF} 0.90, 35°C, 75%RH | 63 |
| Figure 63. Evolution of concentration of crystals, water and API for sample w_{NIF} 0.90, 35°C, 75%RH | 63 |
| Figure 64. Concentration of components in the liquid phase for sample w_{NIF} 0.80, 35°C, 75%RH | 64 |
| Figure 65. Evolution of concentration of crystals, water and API for sample w_{NIF} 0.80, 35°C, 75%RH | 64 |
| Figure 66. Concentration of components in the liquid phase for sample w_{NIF} 0.80, 30°C, 75%RH | 64 |
| Figure 67. Evolution of concentration of crystals, water and API for sample w_{NIF} 0.80, 30°C, 75%RH | 65 |
| Figure 68. Concentration of components in the liquid phase for sample w_{NIF} 0.70, 35°C, 75%RH | 65 |
| Figure 69. Evolution of concentration of crystals, water and API for sample w_{NIF} 0.70, 35°C, 75%RH | 65 |

| | |
|---|----|
| Figure 70. Concentration of components in the liquid phase for sample w_{NIF} 0.90 in Resomer R203s, 40°C, 75%RH..... | 66 |
| Figure 71. Evolution of concentration of crystals, water and API for sample w_{NIF} 0.90 in Resomer R203s, 40°C, 75%RH..... | 66 |
| Figure 72. Concentration of components in the liquid phase for sample w_{NIF} 0.80 in Resomer R203s, 40°C, 75%RH..... | 66 |
| Figure 73. Evolution of concentration of crystals, water and API for sample w_{NIF} 0.80 in Resomer R203s, 40°C, 75%RH..... | 67 |
| Figure 74. Concentration of components in the liquid phase for sample w_{NIF} 0.70 in Resomer R203s, 40°C, 75%RH..... | 67 |
| Figure 75. Evolution of concentration of crystals, water and API for sample w_{NIF} 0.70 in Resomer R203s, 40°C, 75%RH..... | 67 |
| Figure 76. Calibration curve of NIF at 276 nm in acetonitrile..... | 71 |

List of tables

| | |
|--|----|
| Table 1. Thermal properties of the different polymorphs [24]..... | 23 |
| Table 2. Conditions of the experiments in suspension balance..... | 28 |
| Table 3. PC-SAFT API parameter..... | 32 |
| Table 4. Binary interaction parameters..... | 33 |
| Table 5. Degree of crystallinity of the samples by mass balances..... | 44 |
| Table 6. Melting enthalpies obtained by DSC measurements..... | 47 |
| Table 7. Results from UV-Vis measurements..... | 48 |
| Table 8. K coefficients with API weight fraction variation..... | 50 |
| Table 9. K coefficients with relative humidity variation..... | 51 |
| Table 10. K coefficients with temperature variation for w_{NIF} 90%..... | 52 |
| Table 11. K coefficients with temperature variation for w_{NIF} 80%..... | 52 |
| Table 12. K coefficients with temperature variation for w_{NIF} 70%..... | 52 |
| Table 13. K coefficients with polymer variation..... | 53 |
| Table 14. K coefficients with method of preparation variation..... | 54 |
| Table 15. Measurements in the spray drying process..... | 57 |
| Table 16. DSC method..... | 69 |
| Table 17. Data about samples and their DSC measurements..... | 68 |
| Table 18. Recorded absorbances from UV-Vis measurements..... | 70 |

Contents

| | |
|--|-----|
| Declaration of authorship | i |
| Abstract | ii |
| List of symbols | iv |
| List of abbreviations | iv |
| List of figures | v |
| List of tables | vii |
| 1. Aim of the project | 1 |
| 2. Theory | 3 |
| 2.1 Stabilization of APIs in polymeric matrices (solid dispersions) | 3 |
| 2.1.1 Methods of preparation | 4 |
| 2.1.2 Solid state characterization | 7 |
| 2.2 Phase behavior of API/polymer-formulations | 9 |
| 2.3 Influence of humidity on the phase behavior | 13 |
| 2.4 Estimation of crystallinity via mass balances and water sorption | 14 |
| 2.5 Calculation of activity coefficients via PC-SAFT | 16 |
| 2.6 JMAK equation | 19 |
| 3. Materials and experimental methods | 22 |
| 3.1 Materials | 22 |
| 3.2 Experimental methods | 25 |
| 3.2.1 Preparation of formulations via spray drying | 25 |
| 3.2.2 Suspension balance experiments | 26 |
| 3.2.3 Verification of crystallinity via PXRD and DSC | 28 |
| 3.2.5 UV-Vis measurements | 30 |
| 4. Results and discussion | 32 |
| 4.1 Modeling the phase behavior of API/polymer-formulations | 32 |
| 4.2 Predicting the influence of humidity on the phase behavior | 34 |
| 4.3 Results of suspension balance experiments | 36 |
| 4.3.1 Influence of w_{NIF} | 37 |
| 4.3.2 Influence of RH | 38 |
| 4.3.3 Influence of Temperature | 39 |
| 4.3.4 Influence of polymer type | 41 |
| 4.3.5 Influence of the method to prepare the formulation | 42 |
| 4.4 Results of PXRD and DSC-measurements | 46 |

| | |
|--|----|
| 4.5 Results of UV-Vis measurements | 48 |
| 4.6 Determination of Avrami-coefficients..... | 49 |
| 4.6.1 Influence of wNIF | 50 |
| 4.6.2 Influence of RH..... | 51 |
| 4.6.3 Influence of Temperature..... | 52 |
| 4.6.4 Influence of polymer type..... | 53 |
| 4.6.5 Influence of the method to prepare the formulation | 54 |
| 5. Conclusion..... | 55 |
| Appendix | 57 |

1. Aim of the project

Nifedipine (NIF) is a calcium channel blocker, widely used clinically as a coronary vasodilator. Pharmaceutical preparations are available as capsules, tablets, and solutions, and the drug is usually administered orally or intravenously. The drug is practically insoluble in water, and is reported to be highly light sensitive

The current way of administration implicates a number of weaknesses. In fact, NIF is usually provided as solution using liquid oral drug preparation or by cutting a soft gelatin capsule and by squeezing out the fluid content beneath the tongue [1]. This mode of administration can lead to dosage and assimilation variability. The administration of NIF solid dispersions (SD), by using a suitable polymeric carrier, comes out an interesting *modus operandi* in order to progress into a better dose precision, residence time and patient compliance.

The SD method was initially used to ameliorate the dissolution properties and the bioavailability of poorly water soluble drugs by dispersing them into water soluble carriers.

Dissolution deceleration through SD method using water insoluble polymer for the development of controlled release dosage forms has become a field of interest in latest years [2].

The progress of controlled release SD has a great advantage for avoiding the risk of a sudden release of drug; as the structure of the solid dispersion allow a homogeneous dispersion of the drug molecules [2].

Amorphous formulations have attracted considerable attention in the pharmaceutical field. As the molecular structures of drug candidates become increasingly complex, solubility often becomes a limiting factor in dissolution and oral absorption. The use of the amorphous form is a promising strategy to battle these limitations due to its higher free energy and, therefore, higher apparent solubility than its crystalline equivalent. However, such amorphous formulations are metastable and tend to convert spontaneously to the crystalline state.

When crystallization occurs during processing, or during the shelf-life of the pharmaceutical product, bioavailability and product efficacy may be adversely affected. Therefore, an understanding of the crystallization kinetics from the amorphous state and the prediction of physical instability are important in the pharmaceutical industry.

Long term stability tests are imposed by Food and Drug Administration (FDA) at defined Temperature and relative humidity (RH) conditions with which their long term stability is verified and the appropriate polymer and concentration for the formulations are acquired.

The aim of this master thesis is to study the crystallization velocity of NIF formulations from the water content absorbed analyzing different influencing factors: active pharmaceutical ingredient (API) weight fraction, temperature, RH, polymer and the method to prepare the formulation. It brings into focus the characterization of the ternary system (API-polymer-water).

Finally, the predicted crystallization profiles are calculated and compared with the experimental results obtained.

2. Theory

An API is the chemical compound of any formulation which is pharmaceutically active. Some formulations, such as integration treatment, have multiple active ingredients to treat different diseases.

All drugs are made up of two core elements: the API, which is the central ingredient, and the excipient, the substance inside the drug that helps deliver the medication to the desired place within the organism. Excipients are inactive substances, such as polymers, and not chemically active.

According to the U.S. Food and Drug Administration, an API is defined as:

“Any substance or mixture of substances intended to be used in the manufacture of a drug product and that, when used in the production of a drug, becomes an active ingredient in the drug product. Such substances are intended to furnish pharmacological activity or other direct effect in the diagnosis, cure, mitigation, treatment or prevention of disease or to affect the structure and function of the body.” [3].

2.1 Stabilization of APIs in polymeric matrices (solid dispersions)

Amorphous formulations have attracted considerable interest in the pharmaceutical field as a way of improving bioavailability [2,4]. As the molecular structures of drug candidates become increasingly complex, solubility often becomes a limiting factor in dissolution and oral absorption.

The crystalline state is thermodynamically the most stable solid state, and is characterized by both lower solubility and higher chemical stability [30].

When crystallization occurs during processing, or during the useful life of the pharmaceutical product, bioavailability and product efficacy may be adversely affected.

The process of crystallization is known to be composed of two major steps: nucleation and crystal growth, and the rates are generally governed by molecular mobility affecting the diffusion rate of molecules and thermodynamic factors such as the Gibbs free energy and nucleus/amorphous interfacial energy.

Preparation of poorly water-soluble APIs into amorphous forms improves their solubility. However, amorphous solids are often physically metastable because of their high energy state, and crystallization during storage presents a problem.

A promising strategy to improve the dissolution limited bioavailability would be to use the amorphous state and take advantage of the higher solubility of this high free energy state. On the other hand, because amorphous drugs are in a higher free energy state than a corresponding crystalline state, re-crystallization is thermodynamically favored.

The phase behavior of solid dispersions can be extremely complicated, whereby the API can potentially be present in its crystalline state (which may involve one or more polymorphic forms) or as a fully or partially amorphous form. For amorphous solid dispersions, one important aspect of the phase behavior is the miscibility of the amorphous phases of the drug and the polymeric carrier.

2.1.1 Methods of preparation

There are numerous methods to prepare a solid dispersion. Below it is proceed to describe some of them [2]:

Spray drying

Spray drying is a unit operation capable of transforming solutions or suspensions into a solid product. The spray drying technique comprises four basic steps: atomization of the liquid, mixing of the liquid with the drying gas, evaporation of the liquid and separation of the dried particles from the gas [2].

The liquid solution is transferred from the beaker to the nozzle entrance by a pump system. In case of solid dispersion preparation, the used solvents are mostly organics.

As the slurry enters the tower, it is atomized into fine droplets. Partly because of the high surface tension of water and partly because of the hydrophobic/hydrophilic interactions between the amphipathic carrier, the water and the load, the atomized slurry forms micelles.

Several types of atomization devices are available, depending on the type of energy that is involved: centrifugal energy, pressure energy, kinetic energy and vibrations.

All spray dryers use some type of atomizer or spray nozzle to disperse the liquid or slurry into a controlled drop size spray. The most common of these are rotary disk and single-fluid high pressure swirl nozzles.

The small size of the drops (averaging 100 micrometers in diameter) results in a relatively large surface area which dries quickly. As the water dries, the carrier forms a hardened shell around the load. The final product is removed from the gas phase in a cyclone and collected in a cyclone at the end of the process [5]

A general scheme for a spray drying equipment is depicted in the following Figure 1:

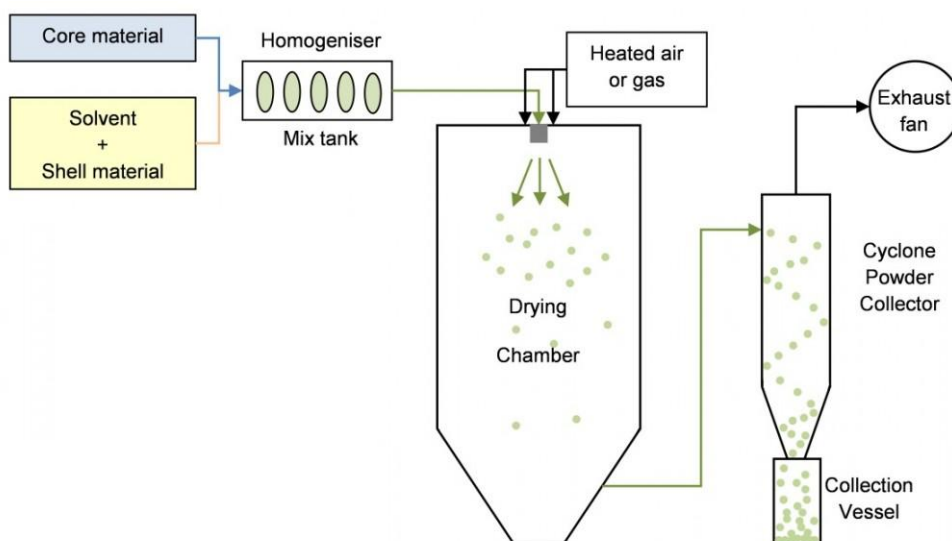


Figure 1. Scheme of spray drying method [6]

Melting method

The melting method involves melting of a physical mixture of drug and carrier to the liquid state followed by cooling until solidification [2]. It is the simplest method which can be used,

one of the advantages is that it is a solvent free method. However, the API and the excipient should be miscible and mixed well [4].

Melting solvent method

The melting solvent technique is a combination of the solvent evaporation method and melting method [2].

It is carried out by the dissolution of the drug in an appropriate solvent and the mixture of this solution with the molten carrier followed by cooling for solidification. The advantage of this method is that it needs inferior temperatures with lesser risk of decomposition of thermolabile drugs than other methods.

Solvent evaporation method

This technique consists of dissolving the drug and excipient simultaneously in a common solvent, followed by the withdrawal of the solvent by evaporation.

Many drugs and carriers cannot be utilized for others methods, such as melting method, due to their high melting points, then they can be used for solvent evaporation method [2].

Hot melt extrusion

The advantages of this technique include lower temperature than other methods and shorter residence time of the drug carrier mixture. The physical mixture of drug and excipient is moved into the heated chamber of extruder at a controlled rate.

Since the physical mixture is carried through heated screws, it is melted, which allows homogeneous mixing. In the last step of the process the melt is shaped in the required form such as granules, pellets, tablets, powder [4].

The following Figure 2 shows a general outline of the process:

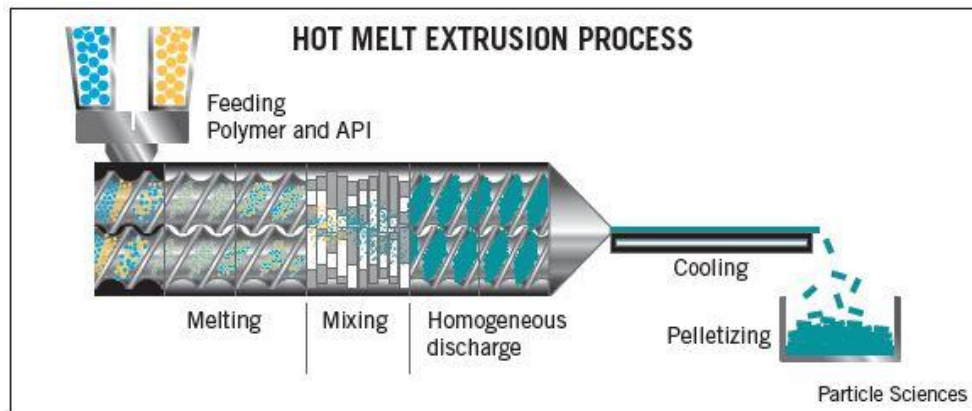


Figure 2 Hot melt extrusion process [7]

Supercritical antisolvent method

It is said a single fluid phase is supercritical when it is above its critical pressure and temperature. Carbon dioxide is the most used supercritical fluid.

Several terms are used according to the technique by which supercritical fluid and solution are mixed: (1) precipitation from supercritical solutions by fast expansion of supercritical solution, (2) precipitation from saturated solution using supercritical fluid as an antisolvent, (3) precipitation from gas saturated solutions [2].

2.1.2 Solid state characterization

Owing to the importance of the nature of solid dispersions, either crystalline or amorphous state, it is needed to verify which state has been achieved both at the beginning and at the end of each experiment.

For this reason, several techniques have been used. These are Powder X-Ray Diffraction (PXRD) and Differential Scanning Calorimetry (DSC) since they are the most generally used techniques to define the solid state. Spectrophotometer has been used in order to measure the real API weight fraction of the formulation.

PXDR is a technique using X-Ray to illustrate the crystalline state of materials. The scattering of X-rays from atoms produce a diffraction pattern that contains information about the atomic structure. Amorphous materials do not produce any significant peak in diffraction pattern, while crystalline materials are completely the opposite as it can be seen in Figures 3 and 4 [8].

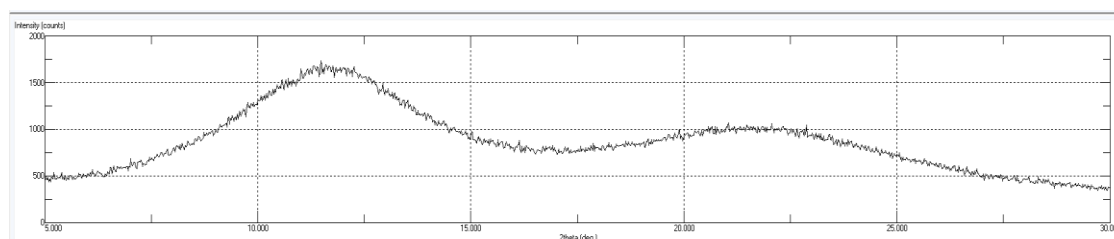


Figure 3. PXDR pattern of an amorphous sample (w_{NIF} 70%)

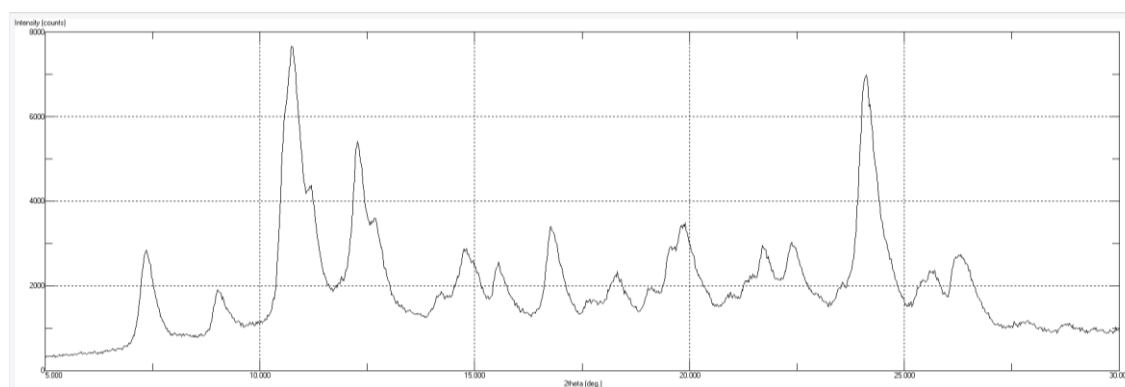


Figure 4. PXDR pattern of a recrystallized sample (w_{NIF} 80%, PVAC350, 40°C, 75%RH) obtained after the suspension balance experiment

DSC is an analytical technique in which the difference in heat flow between a sample and an inert reference is measured as a function of time and temperature as both are subjected to a controlled environment of time and temperature [9].

DSC analyses give information about melting temperature and enthalpy by the study of endothermic peak as illustrated in Figure 5, and its crystallinity composition.

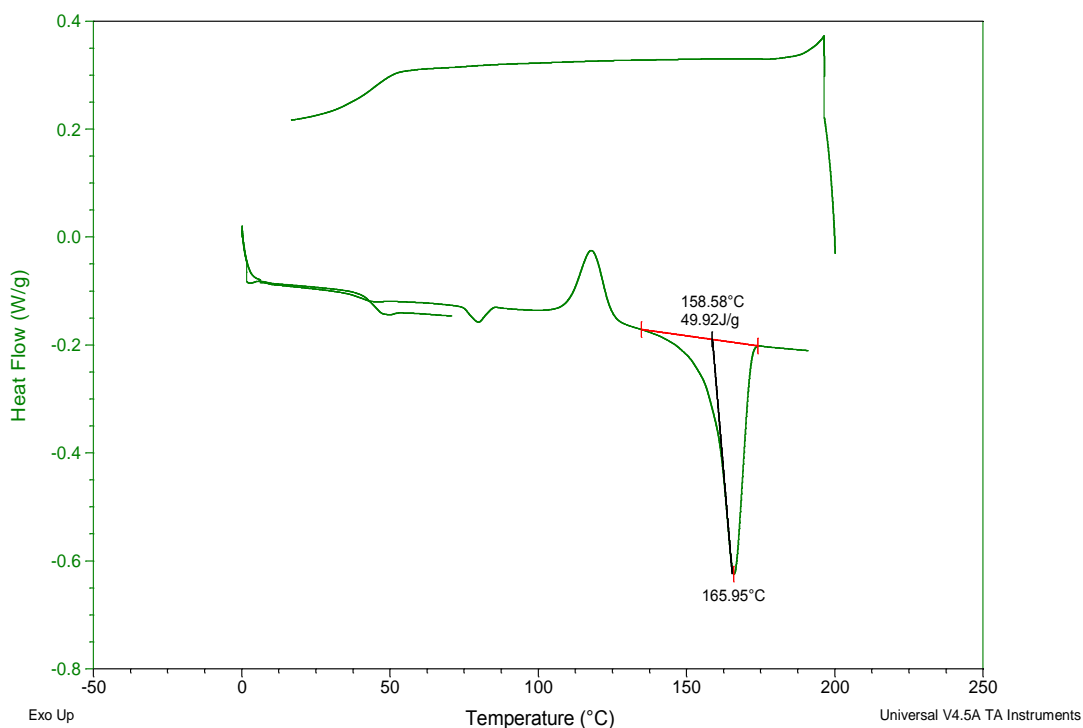


Figure 5. DSC thermogram of NIF/PVAC (w_{NIF} 70%, PVAC, 40°C, 75%RH)

A UV-VIS Spectrophotometer has been used to measure the absorbance at a particular wavelength in order to verify the composition of both components at the end of experiment.

2.2 Phase behavior of API/polymer-formulations

In this section, it will be discussed the phase behavior of API-polymer formulations. The phase behavior of the system depends on the conditions in which the work is being done, thereby different cases can be found.

The knowledge of the phase behavior is of great interest for practical application. When recrystallization or an amorphous phase separation of the API / polymer system is observed, the end of the shelf life of the formulation is achieved.

The stability of the mixture is determined by the solubility. The maximum quantity of API that can be dissolved in the polymer without crystallization is the API solubility in the polymer and thus depends on the phase behavior of the resulting API/polymer formulation.

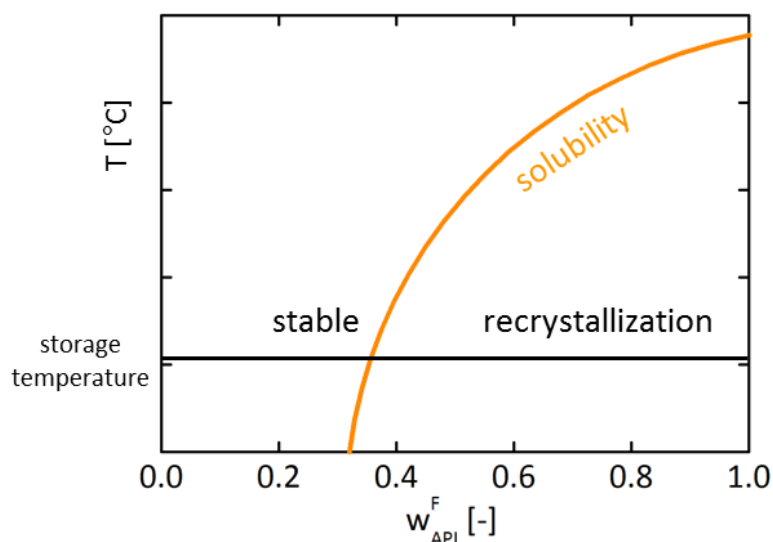


Figure 6. Behavior of solubility against temperature and API weight fraction [10]

As it can be seen in Figure 6, solubility separates two contrasting areas. Below the solubility concentration the API-polymer formulation is stable and at API concentrations higher than the solubility, the system tends to crystallize as it is supersaturated and unstable.

On the other hand, it also affects the miscibility gap between the compounds. Therefore it can be distinguished several zones as it can be seen in Figure 7. The green area (upper area) corresponds to the stable zone in which the system is in amorphous state. In the purple sector (upper inner area of the miscibility curve), it is found two liquid phases corresponding to polymer and water. In the dark orange sector (lower area) within the miscibility gap, it is found two liquid phases as in the previous sector and recrystallization may occur as well. Finally in the light orange area there is recrystallization as the concentration is greater than the solubility [10].

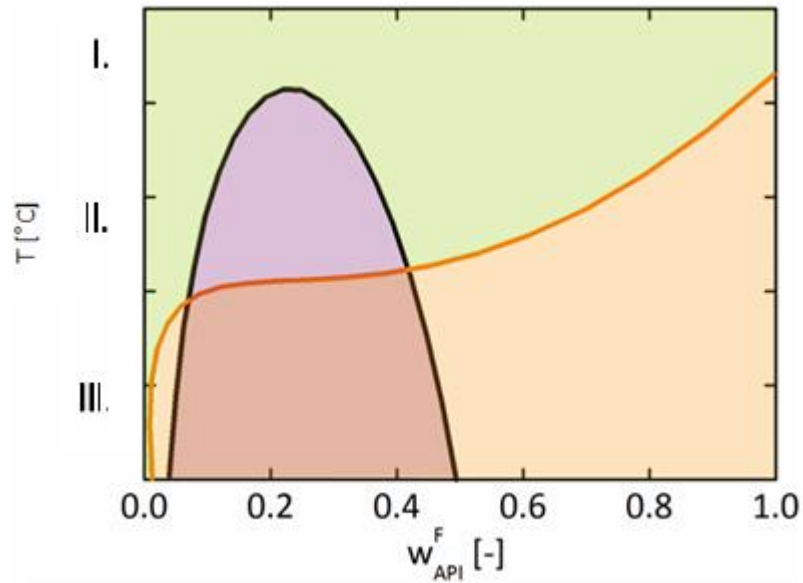


Figure 7. Behavior of solubility and present phases against temperature and weight fraction [10]

If a high API concentration is present, the solubility of the API in the polymer/water mixture is exceeded, the API recrystallizes and a vapor-solid-liquid equilibrium ensues. It is assumed that the vapor phase still consists exclusively of water. In the liquid phase amorphous API and polymer as well as sorbed water are present. The solid phase consists of pure crystalline API. The recrystallization of the API reduces the API concentration in the liquid phase, which in turn affects the water absorption.

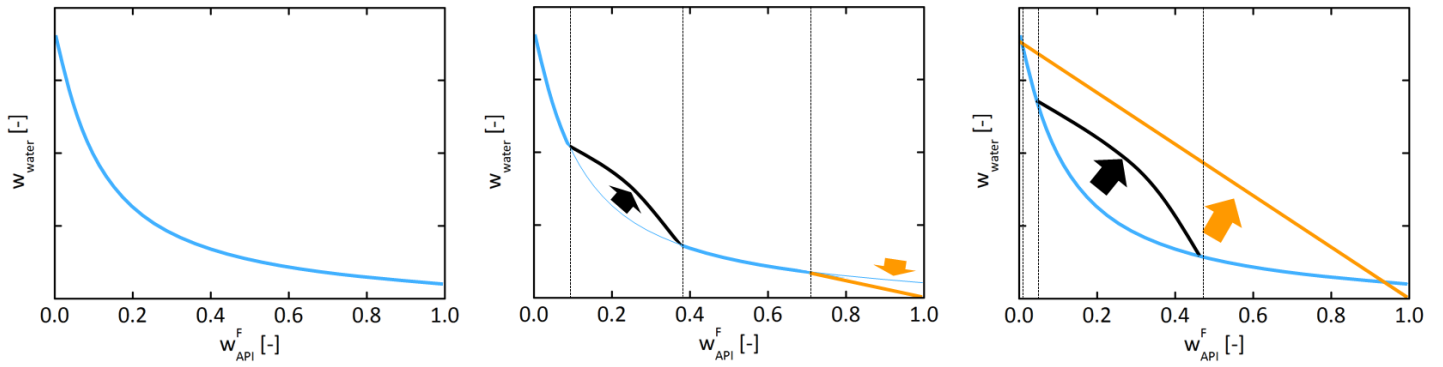


Figure 8. Evolution of water weight fraction: (a) initial curve for amorphous formulation at temperature I, (b) at temperature II, and (c) at temperature III [10]

The evolution of the water weight fraction from the amorphous to crystalline state can be followed in the next Figure 8.

In the next Figure 9, it can be observed the evolution of solubility in this specific case of a Nifedipine-PVAC sample in conditions of 40°C and 75% RH.

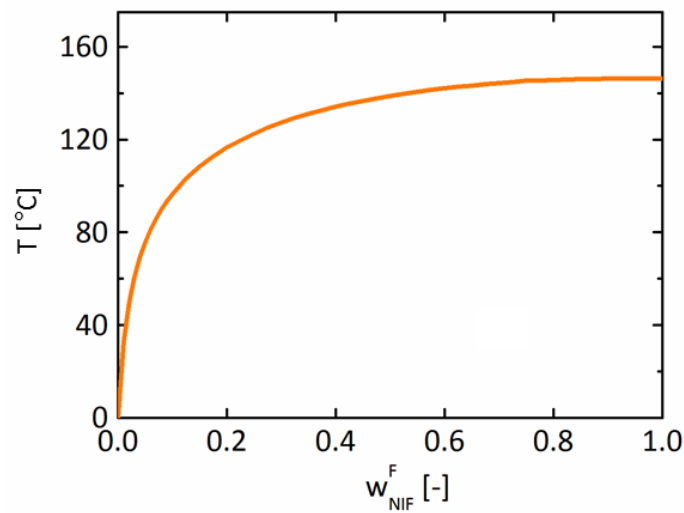


Figure 9. Behavior of NIF solubility [10]

2.3 Influence of humidity on the phase behavior

In this chapter, it will be discussed the effect of humidity in the polymer-API system as it is being studied the crystallization by the water absorbed. Amorphous solid dispersions are prone to absorb water which drives to crystallization of API. Both the API solubility and water sorption depends on type of API and polymer on the formulation, as well as the temperature and the RH [10].

The water sorption of the formulations depends on the physical state of them. Phase transformations can be observed as function of time.

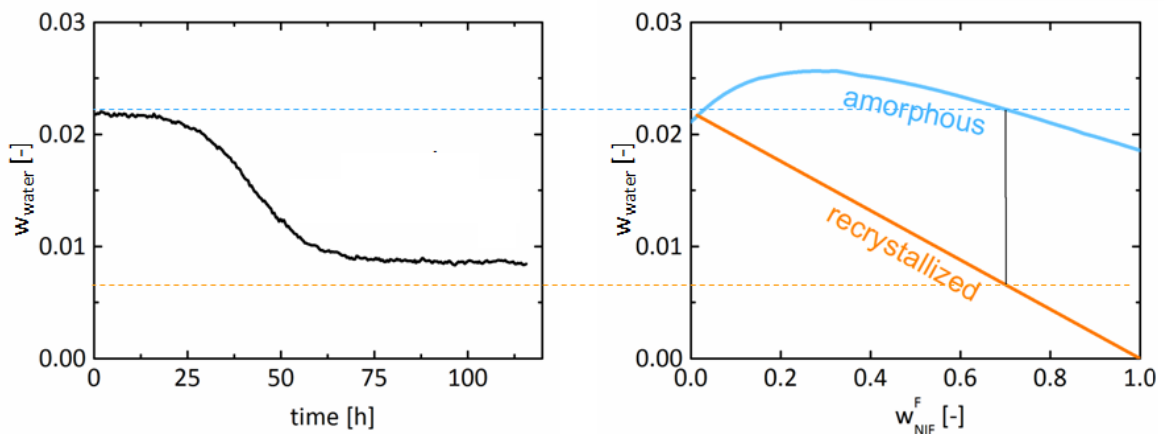


Figure 10. Behavior of water content and phases during crystallization for a w_{NIF} 70% [10]

As it can be seen in the previous Figure 10, the maximum value of water weight fraction corresponds to amorphous nature and as time goes on the sample begins to crystallize until reaching the minimum possible water value [11].

As the relative humidity of the amorphous system was increased, a decrease in the glass transition temperature was noticed indicating an increase in molecular mobility which leads to a faster crystallization [12]

Therefore, on the one hand, water absorbed from the vapor phase induces API crystallization; and on the other hand, the crystallinity of the API/polymer system determines the quantity of water which is absorbed.

2.4 Estimation of crystallinity via mass balances and water sorption

In order to estimate the crystallinity of the sample from the water sorption, obtained from the suspension balance experiments, it is necessary to make use of mass balances and Vapor-Liquid-Equilibrium (VLE) and Solid-Vapor-Liquid-Equilibrium (SVLE).

Regarding to the mass balances, it was required to implement a global mass balance to the whole system and a mass balance to every substance taking into account the two existing phases: solid and liquid.

One assumption taken is that the water is absorbed only by the amorphous liquid phase. The solid phase consists exclusively of crystalline API, polymer and water are insoluble in the API crystal.

Furthermore, the mass of the amorphous polymer in the liquid phase of the water-free system is equal to the mass of polymer in the water-loaded system.

The mass of API in the saturated liquid phase and in the crystalline solid corresponds to the mass of the API in the water-free system.

Global mass balance:

$$m^{total} = m^L + m^S \quad (1)$$

In this expression, m^L and m^S mean the total liquid and solid phase respectively.

Water mass balance:

$$m_W^{total} = m_W^L + m_W^S \quad (2)$$

In which the total water mass is the sum of water mass in the liquid phase and the water mass in the solid phase. This last one is equal to zero, $m_W^S = 0$, due to it was assumed that the solid phase, that is the crystals, is completely composed by NIF.

On the other hand, the liquid water mass depends on the absorbed water weight fraction and the formed crystal percentage per total mass m^S/m_{ges} .

$$m_W^L = \frac{W_{W,ges}}{1 - m^S/m_{ges}} \quad (3)$$

Polymer mass balance:

$$m_{polymer}^{total} = m_{polymer}^L + m_{polymer}^S \quad (4)$$

Where the polymer total mass is equal to the sum of polymer liquid phase mass and the polymer solid phase mass. As it was said before, as it was assumed that the solid phase is completely composed by API, then the polymer mass in the solid phase is zero.

$$m_{polymer}^S = 0 \quad (5)$$

And the polymer liquid phase weight fraction depends on the API and H₂O weight fraction.

$$w_{polymer}^L = 1 - w_{API}^L - w_W^L \quad (6)$$

API mass balance:

$$m_{API}^{total} = m_{API}^L + m_{API}^S = w_{API}^L \cdot m^L + w_{API}^S \cdot m^S \quad (7)$$

In this expression, the API total mass is equal to the addition of API liquid phase mass and API solid phase mass. As it was assumed that the solid phase is completely composed by nifedipine, then $w_{API}^S = 1$.

On the other side, the liquid phase weight fraction depends on the absorbed water and the API water free-liquid phase weight fraction ($w_{API,F}^L$), which was obtained from the VLE.

$$w_{API}^L = \frac{w_{API,F}^L}{1 - w_{W,ges}} \quad (8)$$

2.5 Calculation of activity coefficients via PC-SAFT

The Perturbed-Chain Statistical Associating Fluid Theory (PC-SAFT) is an equation of state designed for modeling mixtures of all types of substances: gases, solvents and polymers.

PC SAFT is satisfactory for the calculation of phase equilibrium and thermodynamic properties of pure components and mixtures. It is found to be more precise comparing to other equation of state (EoS) for correlation of experimental data and more predictive when applied to mixtures. It is very reliable for extrapolations over the regions where parameters were adjusted. Comparison to the original SAFT equation of state reveals significant improvement for both, mixtures of small components and polymer solutions [13].

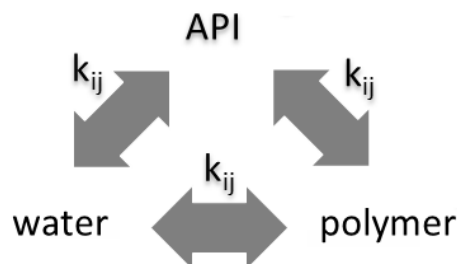


Figure 11. Interaction of the three components of the system

A huge advance in modeling phase behavior of polymer systems has been made during the last years with use of EoS. In many such theories chain-like molecules are modeled as chains of freely-jointed spherical segments.

The PC-SAFT equation of state is based on perturbation theory with the hard chain as reference fluid. The perturbation contributions account for dispersive attractions as well as association interactions and the reduced residual Helmholtz energy [13].

In accordance with this model, molecules are determined by three pure component parameters:

- Attraction parameter ϵ
- Segment number m
- Segment diameter σ

In spite of its clarity, this molecular model considers the vital characteristics of real molecules. Those characteristics are:

- Repulsive interactions
- Non-spherical shape of molecules (chain formation)
- Attractive interactions (dispersion)

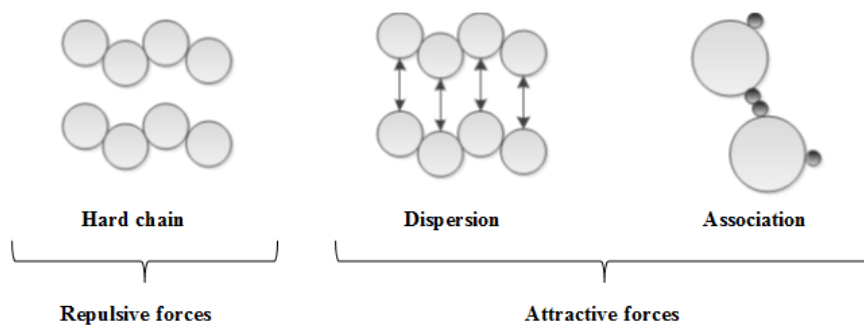


Figure 12. Interaction of the forces involved in the EoS

The hard chain contribution represents the repulsions between the molecules. The attractions of molecules are considered by dispersive interactions and strong hydrogen bonding which exists between the associating molecules.

Therefore, the free residual energy a^{res} is calculated [14]:

$$a^{\text{res}} = a^{\text{hc}} + a^{\text{disp}} + a^{\text{assoc}} \quad (9)$$

Despite considerable work on further developments, one of the most successful models remains the original SAFT equation of state. However, in the dispersion term of the original SAFT model, the chain-like structure of polymer compounds is not taken into account.

In the Perturbed-Chain SAFT equation of state, the dispersive forces are accounted for applying a perturbation theory of second order (Barker and Henderson), using an expression for the radial pair distribution function of a hard-chain reference fluid [13]

For utilization of the PC-SAFT equation of state to real substances, the integral in the dispersion term is replaced by a power series in density, where the coefficients show a simple dependence on segment number.

To characterize an associating substance, the number of association sites as well as their type has to be assigned according to the molecular structure. Five pure component parameters for associating substances have to be identified:

Segment number:

$$\bar{m} = \sum_i x_i \cdot m_i \quad (10)$$

Segment diameter:

$$\sigma_{ij} = \frac{1}{2} \cdot (\sigma_i + \sigma_j) \quad (11)$$

Dispersion energy parameter:

$$u_{ij} = \sqrt{u_i \cdot u_j} \cdot (1 - k_{ij}) \quad (12)$$

Association energy:

$$\varepsilon^{A_i B_j} = \frac{1}{2} \cdot (\varepsilon^{A_i B_i} + \varepsilon^{A_j B_j}) \quad (13)$$

Association volume:

$$K^{A_i B_j} = \sqrt{K^{A_i B_i} + K^{A_j B_j}} \cdot \left(\frac{\sqrt{\sigma_{ii} \cdot \sigma_{jj}}}{0.5 \cdot \sigma_{ii} + \sigma_{jj}} \right)^3 \quad (14)$$

2.6 JMAK equation

In order to represent a model for the kinetics of crystallization, it has been used the Avrami equation. It describes the transformation of one phase from another by the growth of nuclei that are randomly formed in the primary phase.

The Avrami equation is also known as Johnson Mehl Avrami Kolmogorov (JMAK) equation [15].

The crystallization is usually observed to follow a characteristic sigmoidal curve in which it can be differentiated three zones. At the beginning, the crystallization rate is slow as it is the time required for a significant number of nuclei of the new phase to form. The intermediate rate is fast since the nuclei formed in the previous step grow in size. And the final rate is slow

again since most of the compound has been crystallize and there is less material to convert, the particles already existing start to touch each other.

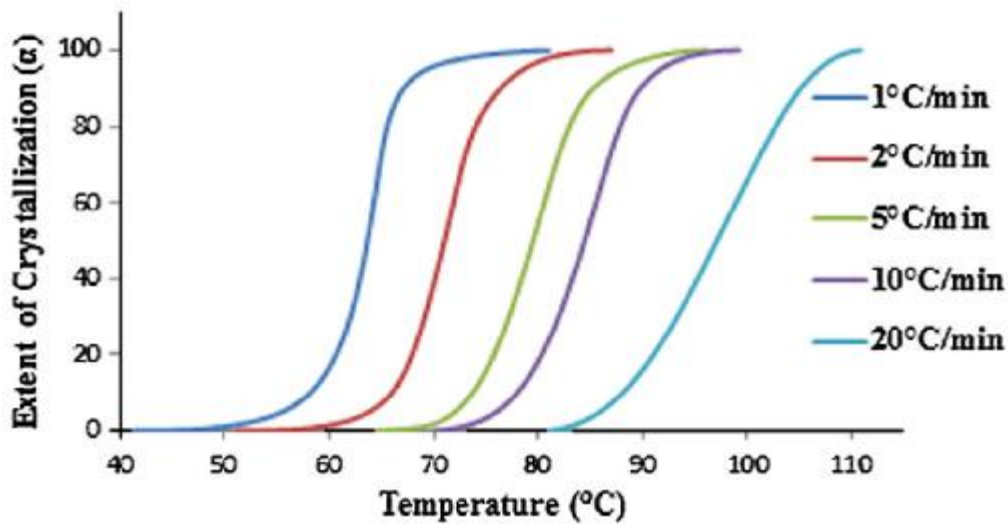


Figure 13. Characteristic sigmoidal curve followed by crystallization [16]

It has been assumed important simplifications to follow Avrami equation [17]:

- Nucleation occurs randomly and homogeneously over the entire untransformed portion of the material.
- Growth rate does not depend on the degree of transformation.
- Growth happens at the same velocity in all directions, the growth is isotropic.

Thus, the number of nuclei is based on the volume, the nucleation rate and the time interval in which it is measured.

$$N = V \dot{N} dt \quad (15)$$

Developing this initial equation, the final equation is reached, the usual form of Avrami equation, which gives the fraction of crystals transformed.

$$y = 1 - \exp(-kt^n) \quad (16)$$

Where $y = \frac{\text{volume transformed}}{\text{total volume}}$

It can also be written as:

$$\ln\left(\ln\left(\frac{1}{1-y}\right)\right) = \ln K + n \ln t \quad (17)$$

This equation allows the estimation of the transformation constants, K and n, as it can be seen in the next Figure 14.

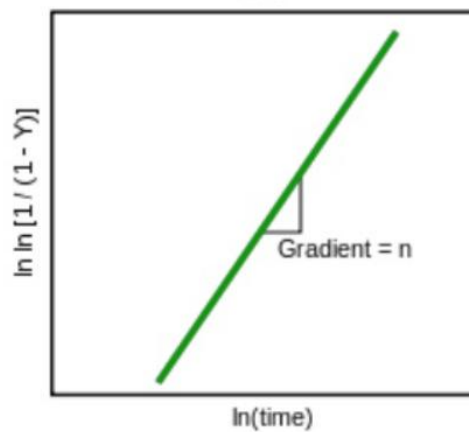


Figure 14. Graph where the slope is the n parameter [17]

K and n are transformation parameters. The n parameter depends on the dimension of the nuclei, and due to the assumptions made earlier, this parameter will be 4 [18].

3. Materials and experimental methods

3.1 Materials

Nifedipine was purchased from Tokyo Chemical Industry CO., LTD. (Tokyo, Japan) with a purity of >98.0%

Poly(vinyl acetate) (PVAC) of a molecular weight of 90.000 g/mol was acquired from Polysciences Inc. (Warrington, PA, USA). Poly(vinyl acetate) (PVAC) of a molecular weight of 350.000 g/mol was purchased from Scientific Polymer Products Inc. (Ontario, NY, USA).

Resomer® R203 S was acquired from Evonik Industries (Darmstadt, Germany).

Acetone with a purity of 99.9%, was purchased from VWR International GmbH (Darmstadt, Germany) was used to prepare the formulations of API and the polymers for spray drying.

NIF is a yellow crystalline substance, practically insoluble in water but soluble in ethanol. It has a molecular weight of 346.3 g/mol and a melting point of 173 °C.

NIF is an antianginal drug belonging to a class of pharmacological agents, the calcium channel blockers. NIF is used to treat hypertension (high blood pressure) and angina (chest pain). It works by relaxing the muscles of your heart and blood vessels. [19].

Nifedipine has the following structural formula [20]:

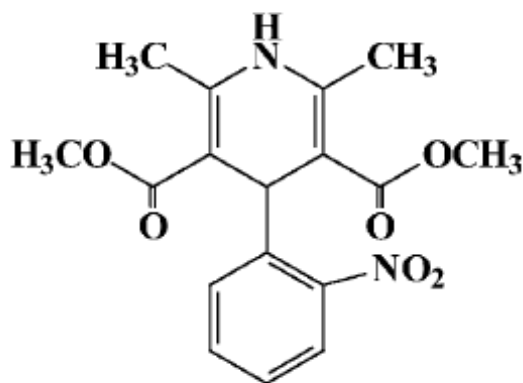


Figure 15. Molecular structure of NIF

Polymorphism, that is the occurrence of chemical compounds characterized by the same structural formula but different crystal forms, is a phenomenon of fundamental importance in organic chemistry as different molecular structure may cause considerable variations in the physical and chemical properties of the compound such as the melting temperature or enthalpy. In the case of nifedipine, three polymorphs have been described: modification III, modification II (or β) and modification I (or α). Only β and α polymorphs are metastable and stable [21,22].

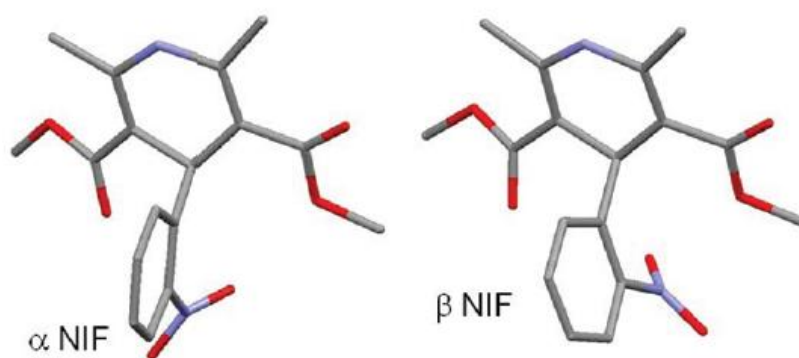


Figure 16. Molecular structure of NIF polymorphs [23]

Table 1. Thermal properties of the different polymorphs [24]

| Properties | α NIF | β NIF |
|--|--------------|-------------|
| Melting temperature ($^{\circ}\text{C}$) | 169-173 | 162-164 |
| Melting enthalpy (J/g) | 104 | 71 |

In order to differentiate the two polymorphs, it was also found the different behavior on heating and cooling. It can be appreciated, in Figure 17, the contract between the shape of the peaks and specially the temperatures at which those peaks occur.

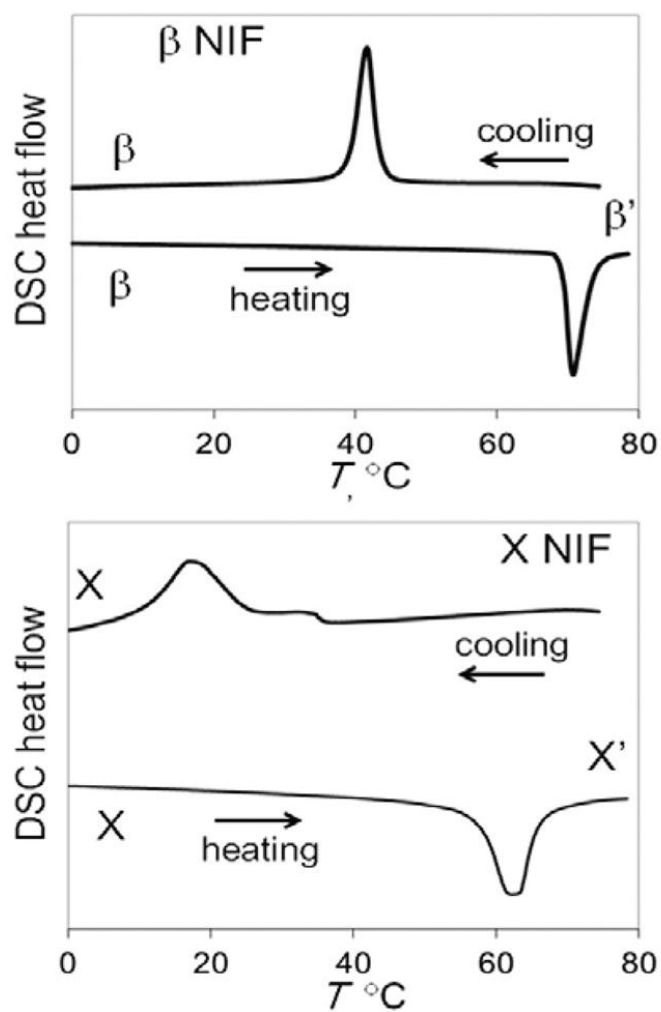


Figure 17. Behavior of the two polymorphs on heating and cooling [23]

According to the X-Ray diffraction, Figure 18 is the pattern of the β polymorph [23], which will be used later to distinguish them as well.

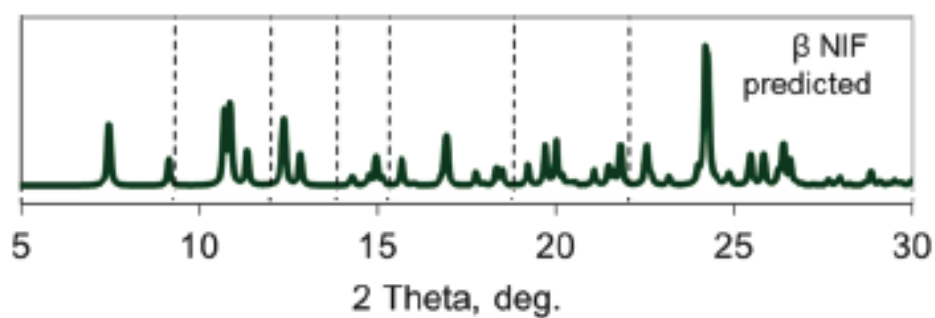


Figure 18. Theoretical NIF pattern by PXRD

3.2 Experimental methods

In the experimental procedure, different stages can be distinguished:

3.2.1 Preparation of formulations via spray drying

The exact quantity of polymer and API contained in each sample was weighted by a balance from Sartorius (Göttingen, Germany) following the selected rates of 70%, 75%, 80%, 85%, 90% NIF. Every sample was 1g.

Next, 100 mL of acetone were added to the mixture to keep a rate of 1/100. Before performing the spray drying, it was needed to stir the solution in order to have it completely dissolved and homogeneous.

In order to perform the solid dispersion preparation, a Mini Spray Dryer B-290 from Büchi has been used.

Firstly, a nitrogen flow was fed into the equipment, so the oxygen inside decreases, to set up inert conditions in the spray dryer. Regarding to aspiration, it was established at a value of 90% of the total capacity of the system.

Once the system was under inert conditions, the heater was started; the selected inlet temperature was 60°C, with which 35-40 °C was reached as outlet temperature. After the selected inlet temperature was achieved, the equipment was drained with pure acetone for 5 minutes to get the drying conditions. The pump rate was set at a point of 30% of its capacity. Afterwards, the spray dryer method started when the pure solvent was switched to the previously prepared solution. At the end of the process, it was switched back to acetone to clean nozzle and tubes.

Finally, the powder resulting from the process was collected with a plastic spoon and stored in a small container.

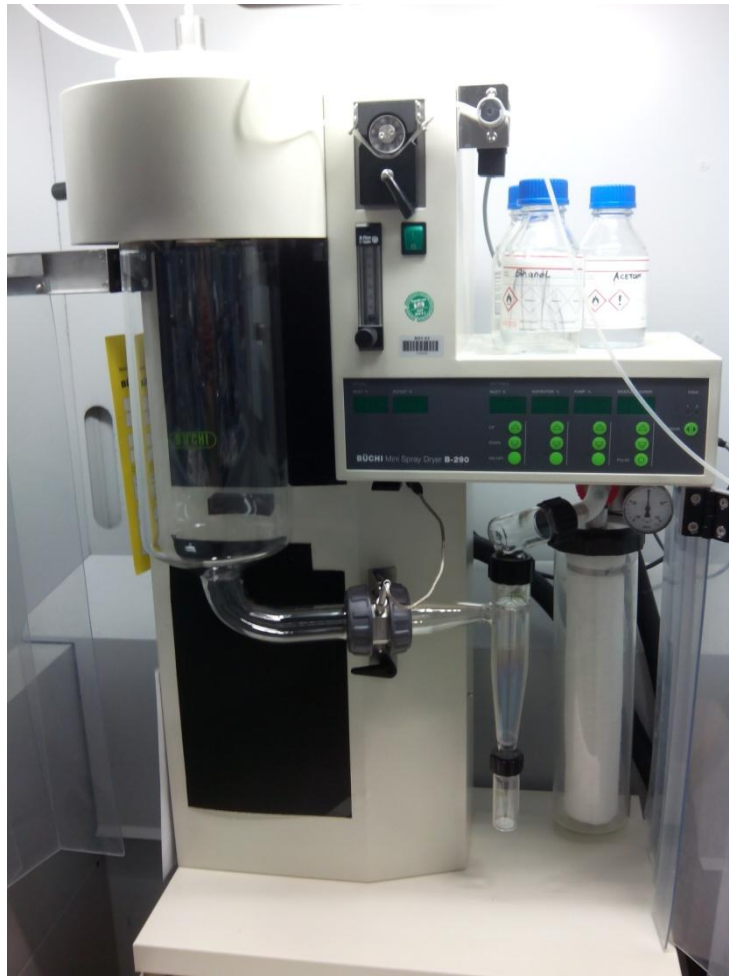


Figure 19. Büchi Mini Spray Dryer B-290 experimental installation

3.2.2 Suspension balance experiments

The suspension balance is the equipment where the water sorption and recrystallization have taken place. Once the solid dispersion was ready from spray drying, the sample was brought here immediately.

Firstly, the solid dispersion was placed in a glass pan which went to the interior of the chamber. Here, the working conditions were vacuum with respect to pressure and the selected temperature during 2 hours, the time needed to reach equilibrium, in order to dry the sample.

Once the equilibrium is achieved, the operating conditions were changed. The pressure was established according to the percentage of required relative humidity and vapor pressure of water at the chosen temperature.

The experiments concluded when the equilibrium was achieved.



Figure 20. Suspension balance experimental installation

In the following table, all the experimental conditions are presented.

Table 2. Conditions of the experiments in suspension balance

| API weight fraction (%) | Polymer | Temperature (°C) | RH (%) |
|-------------------------|----------------|------------------|--------|
| 90 | PVAC | 40 | 75 |
| 80 | PVAC | 40 | 75 |
| 70 | PVAC | 40 | 75 |
| 90 | PVAC | 30 | 75 |
| 80 | PVAC | 35 | 75 |
| 90 | PVAC | 35 | 75 |
| 70 | PVAC | 35 | 75 |
| 80 | PVAC | 40 | 90 |
| 80 | PVAC | 40 | 60 |
| 80 | PVAC | 40 | 75 |
| 80 | PVAC350 | 40 | 75 |
| 80 | PVAC350 | 40 | 75 |
| 90 | PVAC350 | 40 | 75 |
| 80 | Resomer 203s | 40 | 75 |
| 70 | Resomer 203s | 40 | 75 |
| 90 | Resomer 203s | 40 | 75 |
| 85 | PVAC | 40 | 75 |
| 75 | PVAC | 40 | 75 |
| 80 | PVAC (Melting) | 40 | 75 |
| 70 | PVAC (Melting) | 40 | 75 |
| 80 | PVAC | 40 | 75 |
| 80 | PVAC | 30 | 75 |
| 80 | PVAC350 | 40 | 75 |
| 90 | PVAC | 40 | 75 |

3.2.3 Verification of crystallinity via PXRD and DSC

The PXDR measurements have been carried out by Miniflex 600 from Rigaku (Tokyo, Japan) in order to determine if the solid dispersions were amorphous right after the spray drying and crystalline after the suspension balance.

The quantity of the sample to be analyzed was around 5 mg and was kept on a silica area.



Figure 21. Rigaku Miniflex 600 equipment

The DSC measurements have been performed by DSC Q2000 device manufactured by TA Instruments (New Castle, DE, USA) in order to determine thermal characteristics such as degree of crystallinity and melting temperature and enthalpy. These were studied by using TA Universal Analysis software.

For these measurements, an amount of 4-10 mg was weighted and placed in a standard pan.

Some of the adjustments, such as heating rate, were taken from the equipment manual. The procedure used for these measurements can be found in Appendix.



Figure 22. TA Instruments DSC Q-2000 equipment

3.2.5 UV-Vis measurements

In order to verify the final nifedipine concentration of every sample, absorbance was evaluated. The precise concentration in solution was measured by using a BioSpectrometer® from Eppendorf (Hamburg, Germany).

The spectrophotometer was set at a specific wavelength. The absorbance of the nifedipine was measured at 276 nm. The solvent used was acetonitrile. The samples were measured three times in order to have reliable data.



Figure 23. Eppendorf BioSpectrometer equipment

4. Results and discussion

In this section, all the results of the experiments performed are presented. Results from suspension balance, DSC, PXDR and spectrophotometer are shown.

Besides, the influence of every single factor in the solid dispersion is discussed.

4.1 Modeling the phase behavior of API/polymer-formulations

The modeling of the VLEs was determined in this thesis using the PC-SAFT state equilibrium. In order to model the system was necessary the pure substance parameters and binary interaction parameters. The pure substance parameters used for the modeling are listed in Table 3. In addition to the required pure substance parameters, the binary interaction parameters k_{ij} for NIF-water, NIF-PVAC, NIF- Resomer R203s and the polymers with water were also required. The parameters used for modeling are listed in Table 4.

Table 3. PC-SAFT NIF parameter

| | NIF |
|--|-------------|
| Molecular weight | 346.36 |
| Segment number m (mol/g) | 0.023474382 |
| Segment diameter σ_{ij} (Å) | 3.581025 |
| Dispersion energy u_{ij} (K) | 309.4425 |
| Association energy $\varepsilon^{A_i B_j}$ (-) | 1221.582 |
| Association volume $K^{A_i B_j}$ (K) | 0.02 |
| Melting temperature (°C) | 172 |
| Melting enthalpy (J/mol) | 39890 |

Table 4. Binary interaction parameters

| | k_{ij} |
|----------------------------|------------|
| $k_{\text{NIF-water}}$ | 0.011 |
| $k_{\text{NIF-PVAC}}$ | -0.0182717 |
| $k_{\text{water-PVAC}}$ | -0.172 |
| $k_{\text{NIF-Resomer}}$ | 0.009 |
| $k_{\text{water-Resomer}}$ | 0 |

The pure substance and binary parameters presented above arise from adjusting the experimental from [25] to the theoretical model. In the Figure 24 below, it can be seen the adjustment of the data with the parameters presented above.

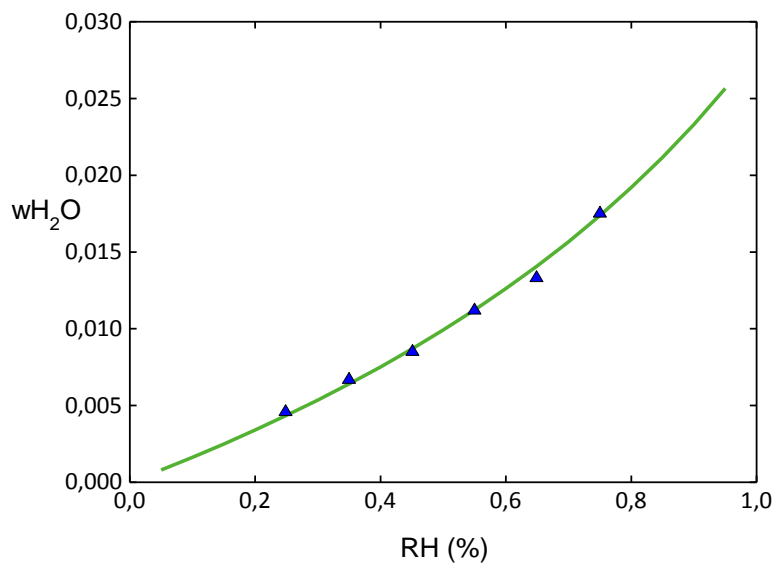


Figure 24. Fitting of the experimental and VLE NIF curves [25]

4.2 Predicting the influence of humidity on the phase behavior

Amorphous API formulations are prone to absorb water from the surrounding atmosphere. This water absorption leads to a crystallization of the NIF, which is a fact to avoid in order to keep the properties and bioavailability achieved with the amorphous state.

For this purpose, it is an important issue to predict the effect of humidity on the system behavior. Therefore it was studied the water sorption of the samples depending on the relative humidity and temperature under which the samples were being tested.

Sorption diagrams for 60%, 75% and 90% of relative humidity are shown in the next Figures 23, 24 and 25.

As it can be observed, there is a vast contrast between the humidities. At a 75% RH, the sample is able to absorb a maximum value of water of 0,024 in the amorphous state, while at 90% RH it is able to assimilate 0.047 of water and at 60% RH a maximum value of 0.015.

The upper line, represented by triangles, corresponds to the water content accepted by the amorphous formulation and the lower line corresponds to the water content accepted by the crystalline formulation. In this way, it is understood the shape of the Figure 10 in which a maximum water value is obtained in the amorphous state and as the crystallization advances the water content decreases.

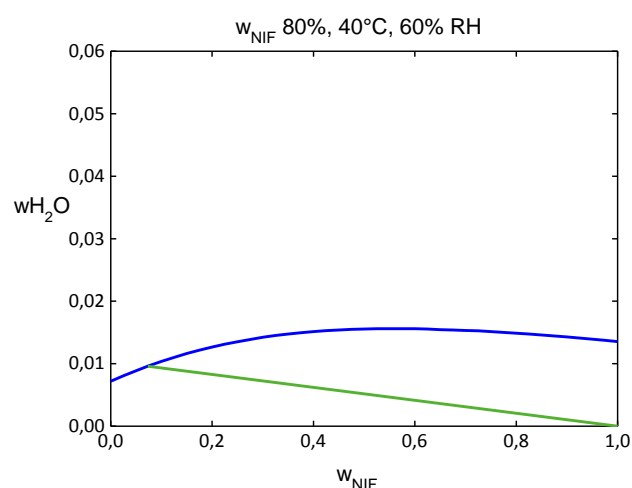


Figure 25. Sorption diagram for sample w_{NIF} 80%, 40°C, 60%RH

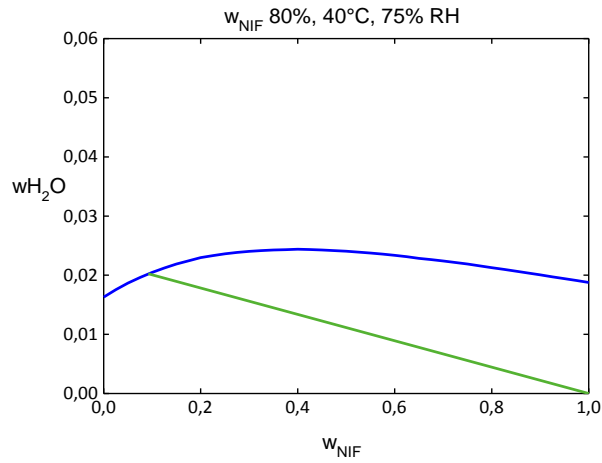


Figure 26. Sorption diagram for sample $w_{NIF} 80\%$, 40°C , $75\% \text{RH}$

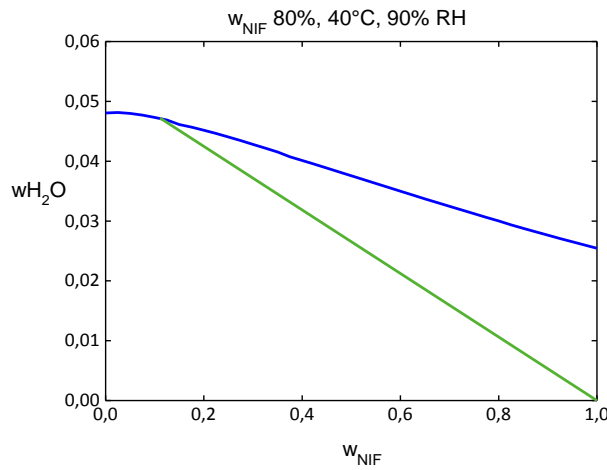


Figure 27. Sorption diagram for sample $w_{NIF} 80\%$, 40°C , $90\% \text{RH}$

Based on these data, it is easily predictable that there will be a sizeable difference both in time required to reach the equilibrium and initial and final water value between the samples.

On the other hand, as it can be seen in the Figures 26 and 27 below, the temperature does not have a substantial effect as the RH. Even though, a higher temperature means a higher water sorption.

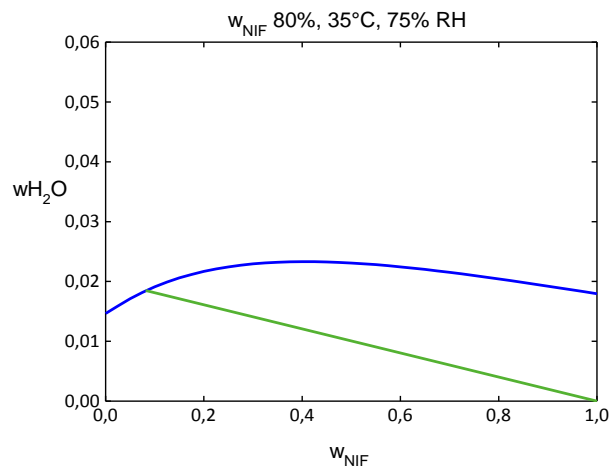


Figure 28. Sorption diagram for sample w_{NIF} 80%, 35°C, 75°RH

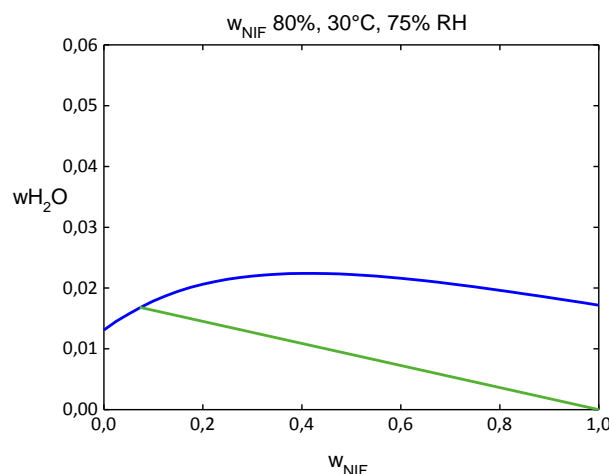


Figure 29. Sorption diagram for sample w_{NIF} 80%, 30°C, 75°RH

4.3 Results of suspension balance experiments

The solid dispersions were placed under the desired conditions of temperature and pressure in the suspension balance.

Firstly, it was decided to set a sample and conditions as a point of reference. This was an NIF weight fraction of 80%, a temperature of 40 °C and a RH of 75%. And in order to guarantee its reproducibility, the experiment was repeated twice. In order to have the same thermodynamic history for all the samples, the same steps were always followed to achieve it.

The data collected from the balance system are weight of the sample and the cell where the powder is; it was also weighted the cell empty. From this weight of the cell and powder and the weight of the cell itself, it can be calculated the water content in the sample.

As it can be seen in Figure 30, both experiments overlap each other reaching the same water content at the beginning and at the end and achieving the equilibrium at the same time.

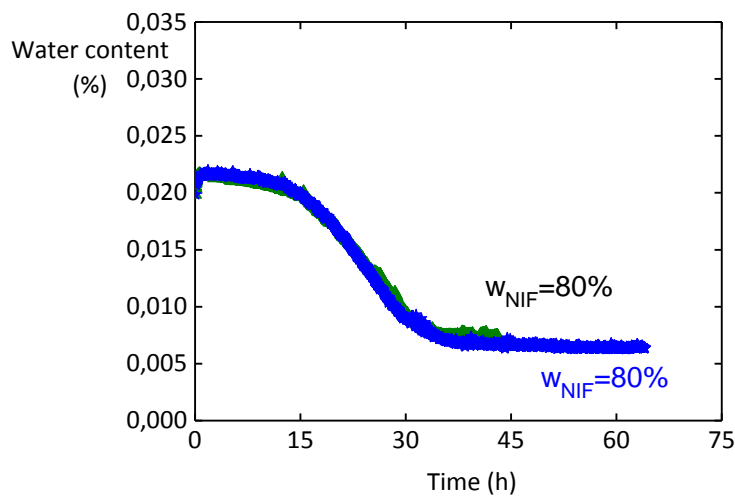


Figure 30. Overlap of the two independent water sorption measurements obtained for $w_{NIF}=0.80$ at 40 °C, 75% RH to check the reproducibility of the experiments

Once this was assured, it was proceeded to study the effect of the influencing factors, always taking these values as reference.

4.3.1 Influence of w_{NIF}

Different weight fractions of the compounds were tested in experiments; these were 90%, 85%, 80%, 75% and 70% of NIF. The temperature and relative humidity were 40°C and 75%, respectively. The results obtained can be seen in Figure 29.

As it can be observed, there is an evolution in every case. The higher concentration of API in the sample, the higher water content is at the beginning and at the ending of the experiment.

And also the lower concentration of API the sample contains, the longer it takes to crystallizes.

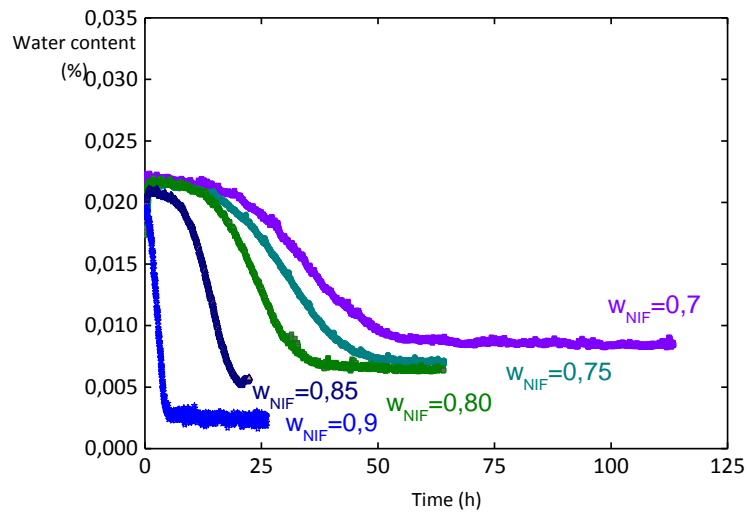


Figure 31. Evolution of water content along the weight fraction

In order to avoid the crystallization of NIF, it will be always to work with a low API concentration. However, it could be the case that with that weight fraction does not reach the recommended dose, in that case it would have to reach a compromise between the weight fraction and the improved properties achieved and the recommended dose. On the other side, future investigations would go in the direction of studying lower API weight fractions.

This can be explained, as it was described in 2.3 Influence of RH on the phase behavior, due to the shape of the curve in Figure 10.

4.3.2 Influence of RH

The effect of the relative humidity in the crystallization was also studied. RH of 90%, 75% and 60% were analyzed. The conditions under which the experiments were performed were: $w_{NIF} = 0.80$, 40°C of temperature and the corresponding RH.

The results obtained are shown in Figure 30.

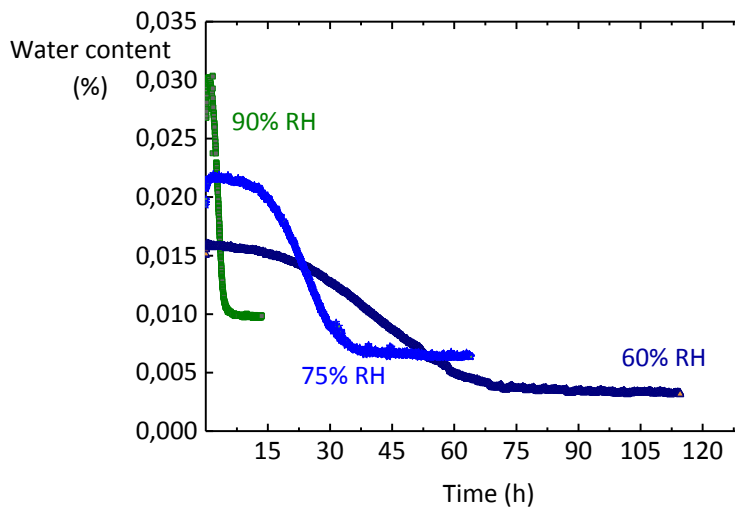


Figure 32. Evolution of water content along RH

As it can be observed in the previous plot, there is a sizable difference between the experiments both in initial and ending water content and time to reach the equilibrium. The higher RH, the higher water absorption, which translates into greater molecular mobility, which leads to greater crystallization [35].

This behavior was also found in [26].

4.3.3 Influence of Temperature

Another influencing factor that has been analyzed is the temperature. The temperatures studied were 30, 35 and 40 °C with NIF weight fractions of 90, 80 and 70%. The RH was 75%. The values acquired are shown in Figure 33,34 and 35

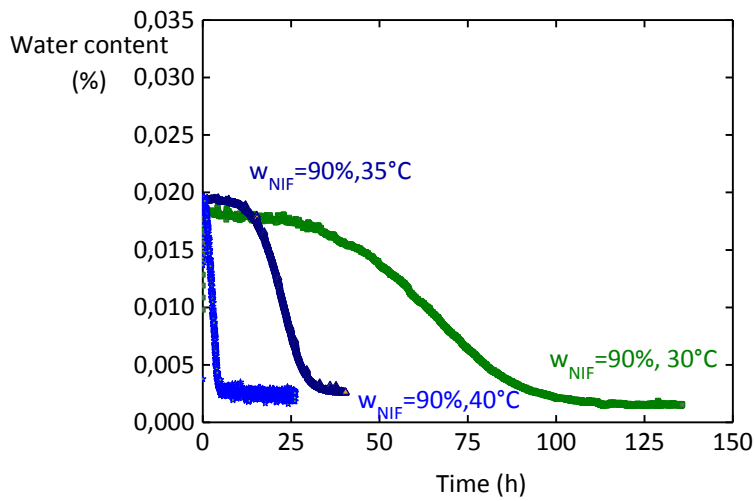


Figure 33. Evolution of water content along temperature for w_{NIF} 90% and 75%RH

As it is observed in Figure 33, the temperature affects the crystallization time. Comparing the temperatures with our reference of 40°C, it is perceived an appreciable difference between them.

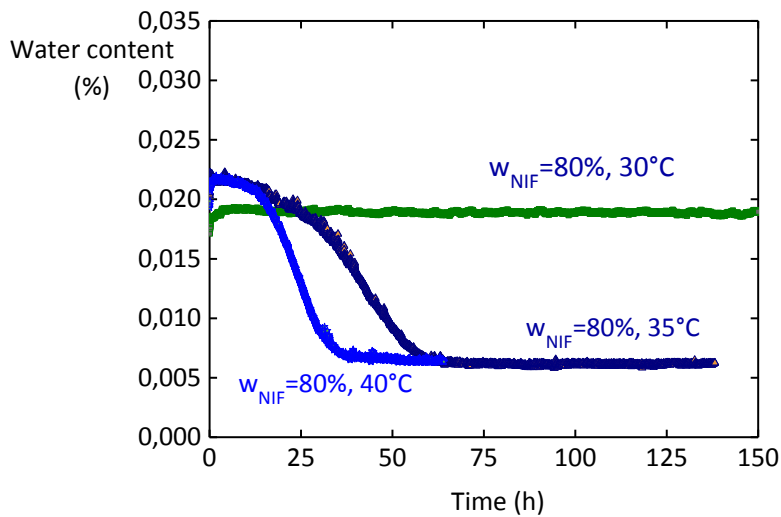


Figure 34. Evolution of water content along temperature for w_{NIF} 80% and 75%RH

In the case of w_{NIF} of 80% shown in Figure 34, the difference is even greater than before as it was reached a week time without the 30 °C curve began to decline.

For the 70% NIF sample observed in Figure 35, it can be seen a considerable difference again. In this NIF weight fraction, the experiment was not performed at 30 °C as it would have been obtained a straight line similar to the 35°C line.

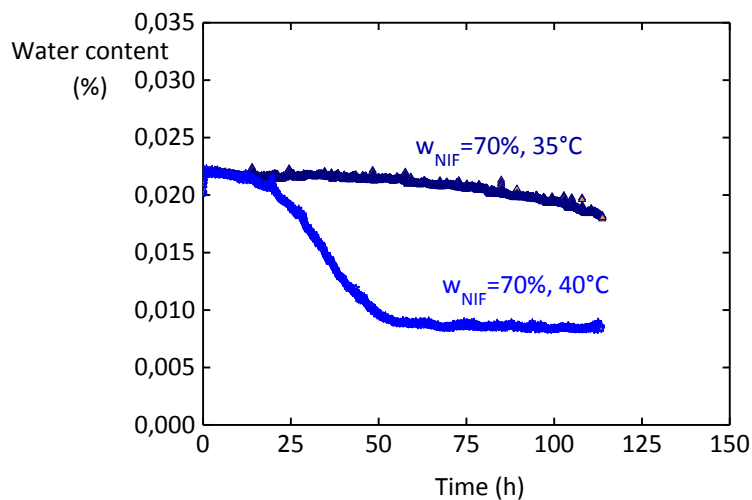


Figure 35. Evolution of water content along temperature for w_{NIF} 70% and 75%RH

According to the results, the temperature conditions in order to prevent crystal formation are the lowest possible temperature.

4.3.4 Influence of polymer type

Another influencing factor studied was the polymer type. It was studied 2 polymers: Resomer® R203 S and PVAC. Regarding to the final polymer, this was investigated 2 different molecular weights. The results can be seen in Figure 36.

As it is shown, there is a contrast between the two polymers in both the crystallization time and water content. The polymer Resomer® R203 S took less time to crystallize and reached lower values of sorbed water.

It can be also noticed the different behavior between the polymer with differing molecular weight although they accomplished the same initial and ending water content.

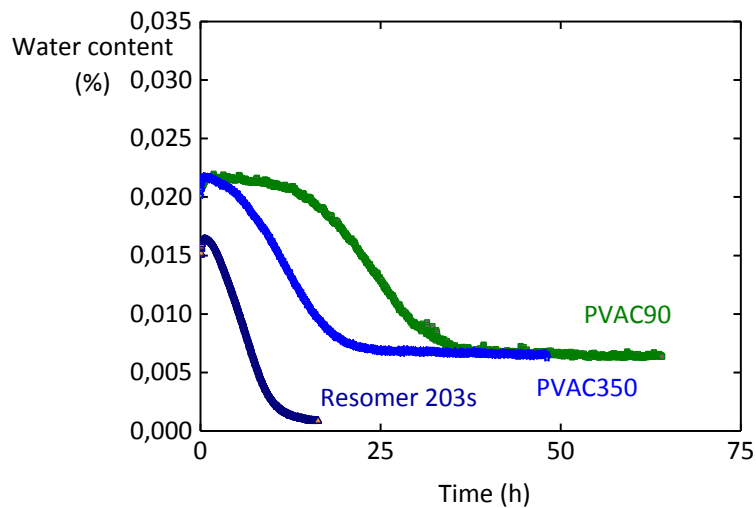


Figure 36. Evolution of water content along polymer for w_{NIF} 80%, 40°C and 75%RH

4.3.5 Influence of the method to prepare the formulation

The last influencing factor studied was the method used in order to prepare the formulation. Two forms of preparation were taken into account: spray drying, as the method used in all the experiments performed, and melting cooling as the method used in real manufacturing.

The results are shown in Figure 37.

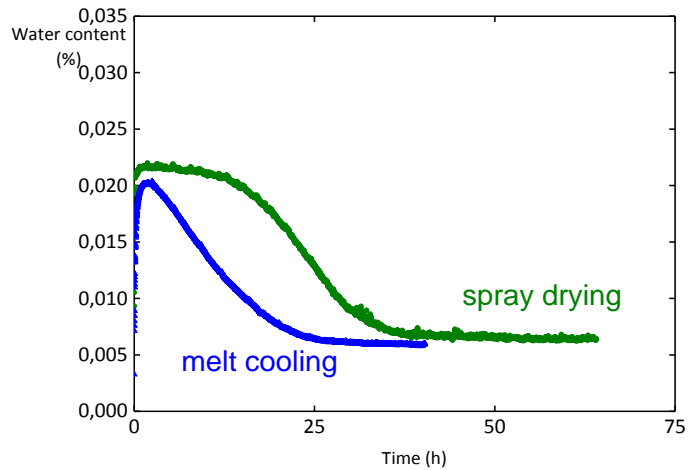


Figure 37. Evolution of water content along the method to prepare the formulation for w_{NIF} 80%, 40°C and 75%RH

In Figure 37, it can be seen that almost the same initial and ending values of water content are achieved.

On the other side, the difference in time to crystallize is appreciable. The time needed for the sample made by melting process is lower than the spray drying sample.

This is an interesting issue since it is question of avoiding crystallization in time, and this melting cooling is the method used in industry.

Calculation of crystallinity via mass balance

Once the suspension balance experiments were done, from the water content data obtained from them, it was proceeded to calculate the degree of crystallinity by mass balances.

In the next Table 5, it can be seen the results of it.

Table 5. Degree of crystallinity of the samples by mass balances

| Polymer | w _{NIF} (%) | T (°C) | RH (%) | w _{Crystals} (%) |
|---------------|----------------------|--------|--------|---------------------------|
| PVAC | 90 | 40 | 75 | 89 |
| PVAC | 80 | 40 | 75 | 73 |
| PVAC | 70 | 40 | 75 | 63 |
| PVAC | 90 | 35 | 75 | 86 |
| PVAC | 80 | 35 | 75 | 72 |
| PVAC | 70 | 35 | 75 | 18 |
| PVAC | 90 | 30 | 75 | 90 |
| PVAC | 80 | 30 | 75 | 6 |
| PVAC | 80 | 40 | 90 | 79 |
| PVAC | 80 | 40 | 60 | 74 |
| PVAC350 | 80 | 40 | 75 | 73 |
| Resomer 203s | 90 | 40 | 75 | 87 |
| Resomer 203s | 80 | 40 | 75 | 82 |
| Resomer 203s | 70 | 40 | 75 | 70 |
| PVAC | 85 | 40 | 75 | 76 |
| PVAC | 75 | 40 | 75 | 69 |
| PVAC Meltcool | 80 | 40 | 75 | 74 |
| PVAC Meltcool | 70 | 40 | 75 | 60 |

As it can be observed in the previous Table 5 the higher degree of crystallinity was reached always with a w_{NIF} of 90%. It is also noted that the way of preparation of the formulation (spray drying or melting-cooling) does not interfere in the crystallinity achieved even though it does interfere in the process of absorbing water.

The progress of the different concentrations in the system can be observed in the next Figure 38 and 39 for the reference sample (w_{NIF} 0.80, 40°C, 75% RH). It is appreciable that the drop of the API in the liquid phase coincides with the increase of crystal growth and at the same time an increase of the polymer concentration in the liquid phase.

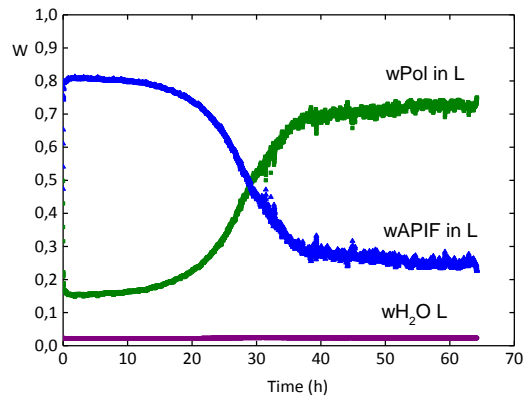


Figure 38. Concentration of compounds in the liquid phase for reference sample (w_{NIF} 80%, 40°C, 75%RH)

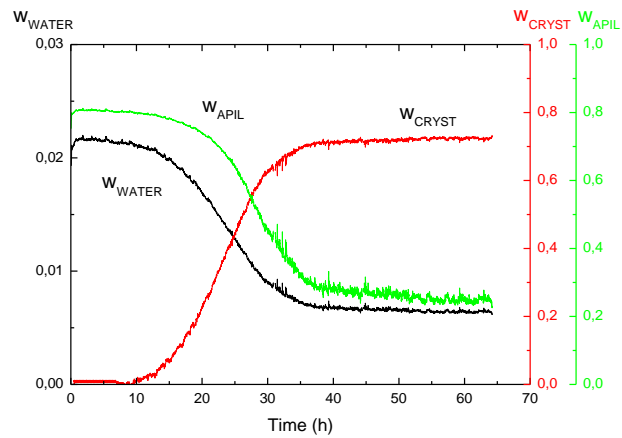


Figure 39. Evolution of concentration of crystals, water and API for reference sample (w_{NIF} 80%, 40°C, 75%RH)

According to what was seen in previous sections, as the water content decreases, the degree of crystallization of the sample increases so the NIF content in the liquid phase decreases, as it can be observed in Figure 39.

The plots of the development of concentrations for the rest of the samples can be seen in Appendix.

4.4 Results of PXRD and DSC-measurements

During this chapter it will be shown the results of the PXRD and DSC measurements. By performing these experiments, it was wanted to guarantee the amorphous state of the sample right after the spray drying and before the experiment in the suspension balance and the crystalline state after the suspension balance. It was also wanted to calculate the melting enthalpy and therefore verify the degree of crystallinity.

In the next Figures 40 and 41, it is shown the results from PXRD in which the amorphous and crystalline states of the reference sample can be seen, that is w_{NIF} of 80%, 40°C and 75% of RH.

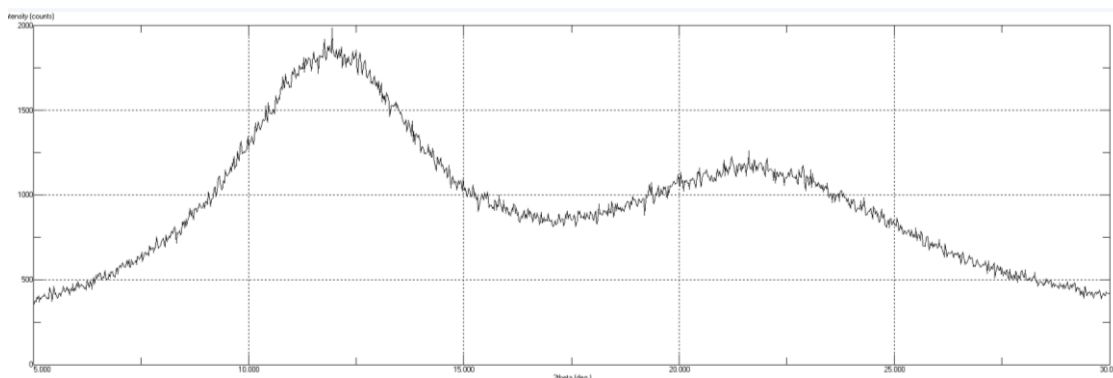


Figure 40. PXRD pattern of amorphous state of sample w_{NIF} 80%

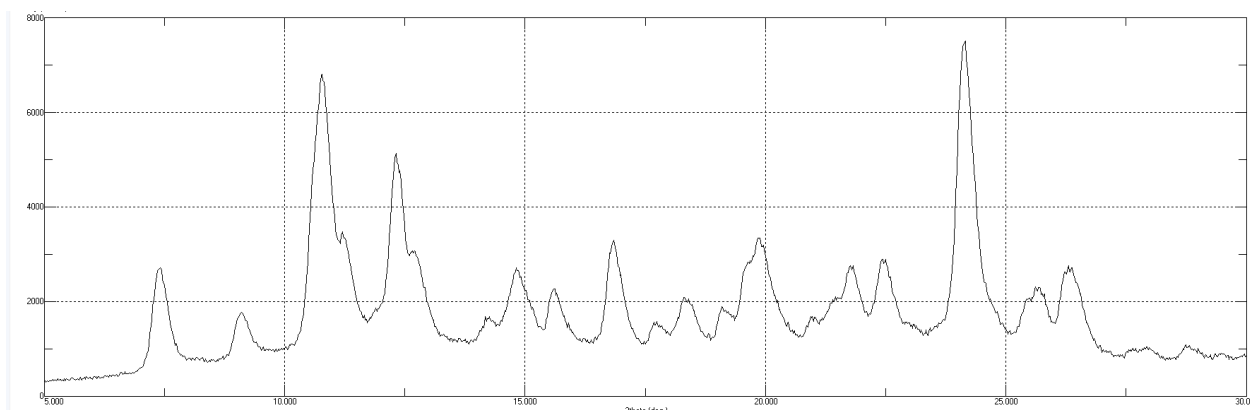


Figure 41. PXRD pattern of crystalline state of sample w_{NIF} 80%, 40°C and 75%RH

According to the PXRD patterns obtained and comparing them to the PXRD patterns from literature (Figure 18) of the different polymorphs of nifedipine, it is proved that the polymorph produced is the β nifedipine when enough time was given. However, when not enough time was given or the NIF weight fraction was 90 or 80%, a mixture of α and β is found. This can be noticed in the differences of crystallinity seen in Table 5 and 6.

The enthalpy of fusion or heat of fusion (Δh_{fus}) is the amount of energy required to make an element at its melting point pass from the solid state to the liquid at constant pressure.

The melting enthalpy is a latent heat since during the process of change of state there is no appreciable change in temperature. Heat is completely inverted in modifying the structure of the material to give mobility to its molecular units.

This melting enthalpy obtained from the literature, as it was said in 3.1 Materials, was compared to the melting enthalpy from the DSC measurements in order to calculate the degree of crystallinity and verify whether the results are as expected.

This data are shown in Table 6 in which it can be seen the operating conditions, the melting enthalpy obtained and the degree of crystallization calculated.

Table 6. Melting enthalpies obtained by DSC measurements

| Polymer | wAPI (%) | T (°C) | RH (%) | Melting enthalpy (J/g) | Degree of crystallinity (%) |
|---------------------|-----------------|---------------|---------------|-------------------------------|------------------------------------|
| PVAC | 90 | 40 | 75 | 70.42 | 67.71 |
| PVAC | 80 | 40 | 75 | 65.15 | 91.76 |
| PVAC | 70 | 40 | 75 | 49.01 | 69.03 |
| PVAC | 90 | 35 | 75 | 72.88 | 70.08 |
| PVAC | 80 | 35 | 75 | 63.40 | 89.30 |
| PVAC | 70 | 35 | 75 | 46.02 | 64.82 |
| PVAC | 90 | 30 | 75 | 81.12 | 78 |
| PVAC | 80 | 40 | 90 | 57.49 | 80.98 |
| PVAC | 80 | 40 | 60 | 33.76 | 47.55 |
| PVAC350 | 80 | 40 | 75 | 58.23 | 82.02 |
| Resomer 203s | 90 | 40 | 75 | 82.38 | 79.21 |
| Resomer 203s | 80 | 40 | 75 | 63.95 | 90.07 |
| Resomer 203s | 70 | 40 | 75 | 49.33 | 69.48 |

4.5 Results of UV-Vis measurements

After performing the experiments, it was measured the homogeneity of the samples by spectrophotometry. As the distribution of the concentration of the powder in a solid dispersion is not certainly ideal owing to possible interferences during the preparation, formation or experiment, it is necessary to calculate the homogeneity of each sample.

The results of the measurements are shown in Table 7.

Table 7. Results from UV-Vis measurements

| Sample | w_{API} (from UV-VIS) (%) |
|--|--|
| wNIF 90, 35°C, 75%RH | 73.58 |
| wNIF 90, 40°C, 75%RH | 90.07 |
| wNIF 90, Resomer R203s, 40°C, 75%RH | 77.54 |
| wNIF 90, PVAC350, 35°C, 75%RH | 72.98 |
| wNIF 85, 40°C, 75%RH | 82.68 |
| wNIF 80, 40°C, 75%RH | 78.99 |
| wNIF 80, PVAC350, 40°C, 75%RH | 63.53 |
| wNIF 80, Resomer R203s, 40°C, 75%RH | 77.09 |
| wNIF 80, Melting-Cooling, 40°C, 75%RH | 82.55 |
| wNIF 80, Melting-Cooling, 40°C, 75%RH | 77.60 |
| wNIF 80, PVAC350, 40°C, 75%RH | 82.42 |
| wNIF 80, 40°C, 75%RH | 79.77 |
| wNIF 80, 40°C, 75%RH | 76.30 |
| wNIF 80, 40°C, 60%RH | 71.39 |
| wNIF 75, 40°C, 75%RH | 73.48 |
| wNIF 70, 40°C, 75%RH | 56.84 |
| wNIF 70, 40°C, 75%RH | 59.10 |
| wNIF 70, Melting-Cooling, 40°C, 75%RH | 73.98 |
| wNIF 70, Resomer R203s, 40°C, 75%RH | 66.07 |

As it can be seen, most of the samples fulfill the API concentration weighted in at the beginning of the experiments.

The absorbances and the calibration curve are in the Appendixes.

4.6 Determination of Avrami-coefficients

In this chapter it will be discussed the coefficients required to fit the experimental curve with the theoretical curve from Avrami equation. As it has been said in a previous section 4.3 Results of suspension balance experiments, a complete crystallization was not achieved in any case, nonetheless the setting of the parameters in all cases is good.

In the next Figure 42, it can be seen how the two curves in the standard case fit together. This has been done for every experiment and the results appear in Appendix. The green curve corresponds to the theoretical curve and the blue one to the experimental.

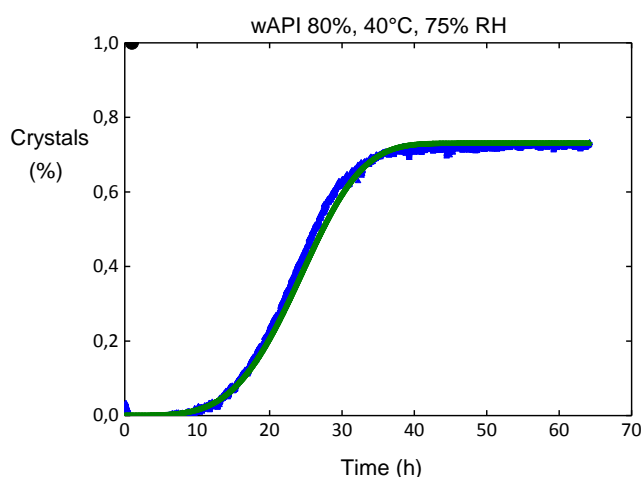


Figure 42. Coupling of the experimental curve and Avrami theoretical curve

Among the parameters to adjust, the n coefficient was set to be constant and equal to 4 as it represents a crystal growth in three dimensions. The K coefficient was variable in every experiment.

4.6.1 Influence of w_{NIF}

The effect on the K coefficient because of the NIF weight fraction can be observed in the next Tables 8. The higher API weight fraction on the sample, the higher the K parameters are. This is because the K parameter has a directly influence in the speed to reach the equilibrium. Therefore, higher API weight fraction means less time to achieve the equilibrium, which means higher K parameter.

Table 8. K coefficients with API weight fraction variation

| w_{NIF} | K parameter |
|-----------|-------------|
| 90 | 1.16E-02 |
| 85 | 2.39E-05 |
| 80 | 2.05E-06 |
| 75 | 9.46E-07 |
| 70 | 6.32E-07 |

It is noted an exponential behavior on the coefficient as it can be observed in the next Figure 43.

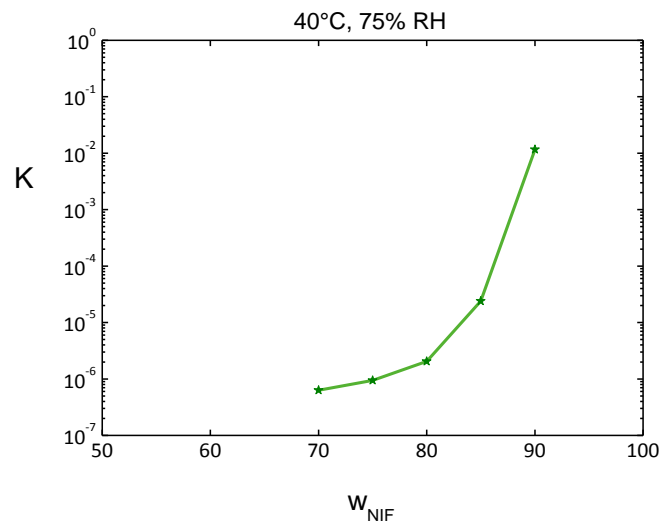


Figure 43. K coefficient behavior with API weight fraction

4.6.2 Influence of RH

Regarding to the effect of relative humidity on the Avrami parameters, it is noted again an exponential behavior as it occurs in the study of weight fraction. This performance can be seen in Figure 44.

The higher relative humidity under which the experiment was carried out, the higher the K parameters are.

Table 9. K coefficients with relative humidity variation

| Relative Humidity | K parameter |
|-------------------|-------------|
| 60 | 2.20E-07 |
| 75 | 2.05E-06 |
| 90 | 1.00E-02 |

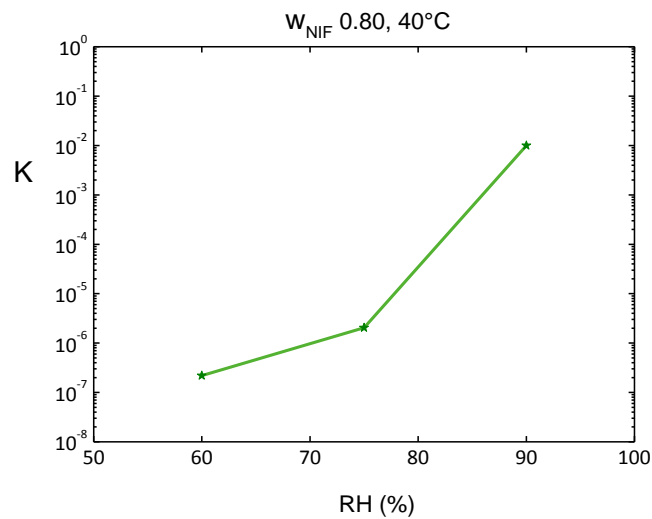


Figure 44. K coefficient behavior with relative humidity

4.6.3 Influence of Temperature

Another influencing factor studied was the temperature and the experimental K coefficients collected can be seen in Figure 45. In that image, it is noted an exponential conduct as in the previous cases.

The higher temperature under which the experiment was carried out, the higher the K parameters are.

Table 10. K coefficients with temperature variation for w_{NIF} 90%

| Temperature (°C) | K parameter |
|-------------------------|--------------------|
| 30 | 4.50E-08 |
| 35 | 2.97E-06 |
| 40 | 1.16E-02 |

Table 11. K coefficients with temperature variation for w_{NIF} 80%

| Temperature (°C) | K parameter |
|-------------------------|--------------------|
| 35 | 2.70E-07 |
| 40 | 2.05E-06 |

Table 12. K coefficients with temperature variation for w_{NIF} 70%

| Temperature (°C) | K parameter |
|-------------------------|--------------------|
| 35 | 6.32E-07 |
| 40 | 2.05E-06 |

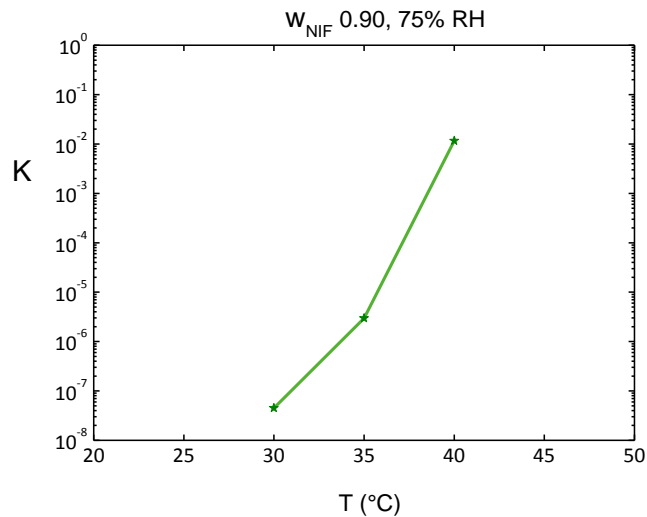


Figure 45. *K* coefficient behavior as function of temperature

This in line with expectations, that is to say, the higher the temperature was in the experiments, the lower time was required to fully recrystallize so that it was expected to have a greater coefficient.

4.6.4 Influence of polymer type

With respect to the effect of the polymer which has been used, it was studied the two polymers presented before: PVAC and Resomer. As it was seen in section 4.3, there is a difference in the time of crystallization between the two polymers, what it was also brought to the *K* parameters. The less time to crystallize, the lower *K* coefficient is.

Regarding the operating conditions, the NIF weight fraction was 80%, the temperature was 40 °C and the RH was 75%.

Table 13. *K* coefficients with polymer variation

| Polymer | K parameter |
|---------------|--------------------|
| Resomer R203s | 5.02E-04 |
| PVAC | 2.05E-06 |

4.6.5 Influence of the method to prepare the formulation

About the modeling by Avrami according to the preparation of the formulation, it can be said that the value is the expected in the sense that is lower than the one obtained from the spray drying as the time required to crystallize is also lower.

The two methods of preparing the formulation studied were spray drying and melting method. Regarding the operating conditions, these were w_{NIF} 80%, 40 °C and 75% RH.

Table 14. K coefficients with method of preparation variation

| Method of preparation | K parameter |
|------------------------------|--------------------|
| Melting method | 3.08E-05 |
| Spray drying | 2.05E-06 |

5. Conclusion

The aim of this project was to study the crystallization of the NIF by observing the water content absorbed and analyzing different influencing factors as NIF weight fraction, temperature, RH, polymer and method to prepare the formulation.

From the resulting data obtained from the study of them, several conclusions have been reached.

First of all, in no case complete crystallization has been achieved. This may be due to a lack of sufficient time to accomplish it.

After spray drying or melting method, the results show that the solid dispersions were totally amorphous. Both the suspension balance experiments and DSC and PXRD measurements have proven to be perfect instruments to study the crystallization of API.

About the NIF polymorphs which are formed, it has been noted that β NIF is the predominantly formed, especially with API weight fraction of 70% and enough time to reach the equilibrium and crystallize. It can be also recognized a mixture of α and β nifedipine when the NIF weight fraction is 90% and 80%.

The Avrami equation has proved its validity to model the behavior followed by the crystallization. The parameters obtained agree with the results achieved from the suspension balance experiments. It has been shown that the assumption of n parameter equal to 4, which is crystal growth in 3 dimensions, is correct.

With respect to the influencing factors studied, some conclusions have come to the fore.

According to the API weight fraction, the lower API concentration the sample contains, the longer it takes to crystallize. The higher concentration of API in the sample, the higher water content is at the beginning and at the ending of the experiment. It could be the case that with that weight fraction does not reach the recommended dose, in that case it would have to reach a compromise between the weight fraction and the improved properties achieved and the recommended dose. On the other side, future investigations would go in the direction of studying lower API weight fractions.

In terms of relative humidity, a huge difference occurs among the several relative humidities that have been implemented. These differences translate into variations in the time required to reach the equilibrium and crystallize and the initial and final water content.

Regarding to the temperature, the lower temperature under the sample is at, the longer it takes to crystallize. Thereby, in order to avoid crystallization, it is necessary to store under a minimum temperature.

In respect of the method to prepare the formulation, differences in time to crystallize emerged. Thus, the time needed for the melting method, the method normally used in industry, is less than the time required for spray drying method. In this manner, in order to avoid crystallization, it might be considered a way to use and optimize the spray drying method on a large scale.

Respecting the polymer used in the formulation, it was noticed that PVAC retarded the time to crystallize so that it better fulfills the purpose of avoiding crystallization than Resomer R203s. In further investigations, more polymers will have to be studied in order to find the optimum.

Appendix

Preparation of formulations via spray drying

Table 15. Measurements in the spray drying process

| Weight NIF (g) | Weight polymer (g) | Polymer | Tin (°C) | Tout (°C) |
|----------------|--------------------|--------------|----------|-----------|
| 0.4491 | 0.0497 | PVAC | 60 | 37 |
| 0.3991 | 0.1005 | PVAC | 60 | 33 |
| 0.7025 | 0.3002 | PVAC | 60 | 41 |
| 1.2075 | 0.8014 | PVAC | 60 | 39 |
| 0.9079 | 0.1002 | PVAC | 60 | 38 |
| 0.8071 | 0.1995 | PVAC | 60 | 38 |
| 0.9014 | 0.1014 | PVAC | 60 | 37 |
| 0.7054 | 0.3064 | PVAC | 60 | 37 |
| 0.8038 | 0.2003 | PVAC | 60 | 39 |
| 0.8043 | 0.2002 | PVAC | 60 | 37 |
| 0.7990 | 0.1995 | PVAC | 60 | 35 |
| 0.8010 | 0.1995 | PVAC350 | 60 | 35 |
| 0.8028 | 0.2012 | PVAC350 | 60 | 39 |
| 0.8033 | 0.2024 | PVAC350 | 60 | 37 |
| 0.9038 | 0.1038 | PVAC350 | 60 | 38 |
| 0.8140 | 0.2001 | Resomer 203s | 60 | 40 |
| 0.7060 | 0.3006 | Resomer 203s | 60 | 40 |
| 0.9071 | 0.1009 | Resomer 203s | 60 | 39 |
| 0.9071 | 0.1017 | Resomer 203s | 60 | 39 |
| 0.8567 | 0.1585 | PVAC | 60 | 36 |
| 0.7506 | 0.2518 | PVAC | 60 | 36 |
| 0.8026 | 0.2018 | PVAC | 60 | 36 |
| 0.8016 | 0.2016 | PVAC | 60 | 35 |
| 0.8047 | 0.2023 | PVAC350 | 60 | 37 |
| 0.9015 | 0.1007 | PVAC | 60 | 39 |

Calculation of crystallinity via mass balance

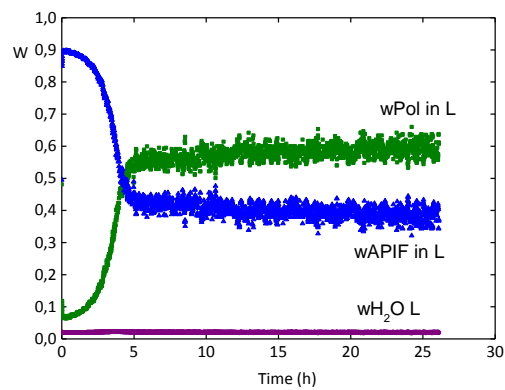


Figure 46. Concentration of components in the liquid phase for sample $w_{NIF} 0.90$, 40°C , $75\%RH$

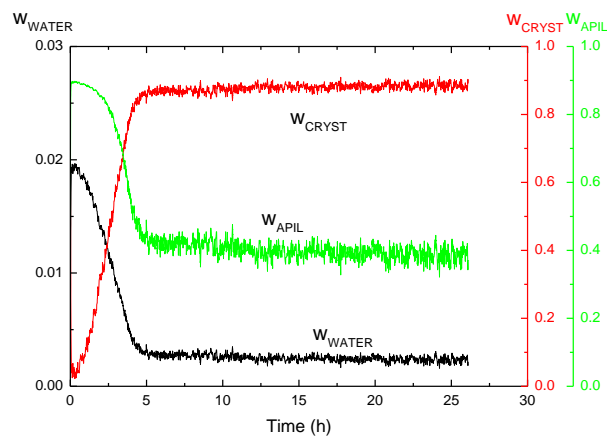


Figure 47. Evolution of concentration of crystals, water and API for sample $w_{NIF} 0.90$, 40°C , $75\%RH$

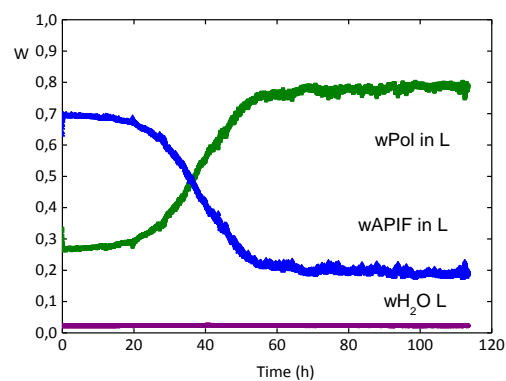


Figure 48. Concentration of components in the liquid phase for sample $w_{NIF} 0.70$, 40°C , $75\%RH$

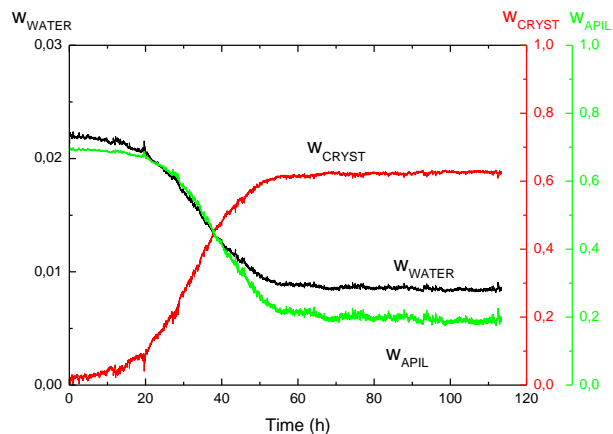


Figure 49. Evolution of concentration of crystals, water and API for sample $w_{NIF} 0.70$, $40^{\circ}C$, $75\%RH$

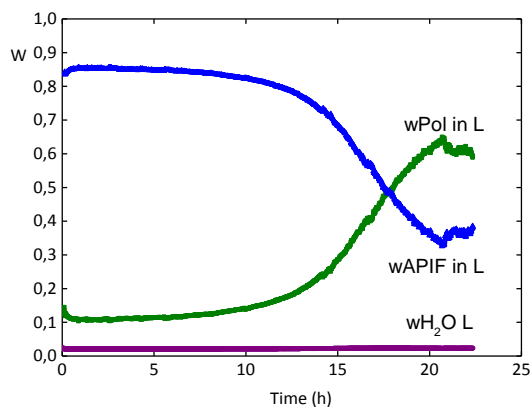


Figure 50. Concentration of components in the liquid phase for sample $w_{NIF} 0.85$, $40^{\circ}C$, $75\%RH$

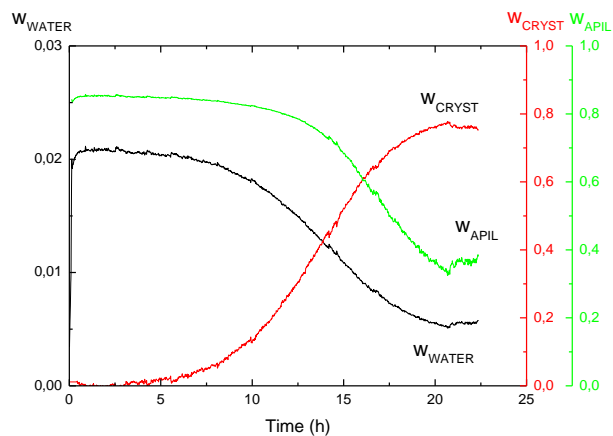


Figure 51. Evolution of concentration of crystals, water and API for sample $w_{NIF} 0.85$, $40^{\circ}C$, $75\%RH$

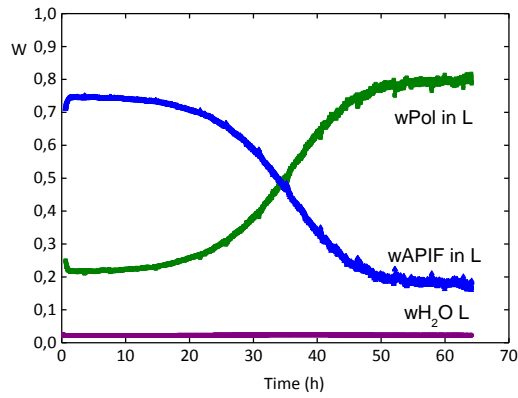


Figure 52. Concentration of components in the liquid phase for sample $w_{NIF} 0.75$, 40°C , $75\%RH$

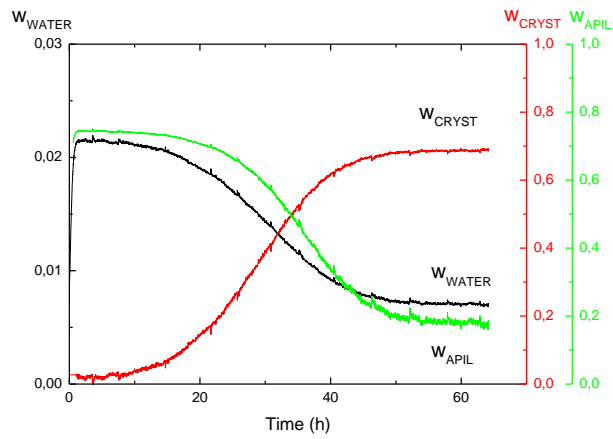


Figure 53. Evolution of concentration of crystals, water and API for sample $w_{NIF} 0.75$, 40°C , $75\%RH$

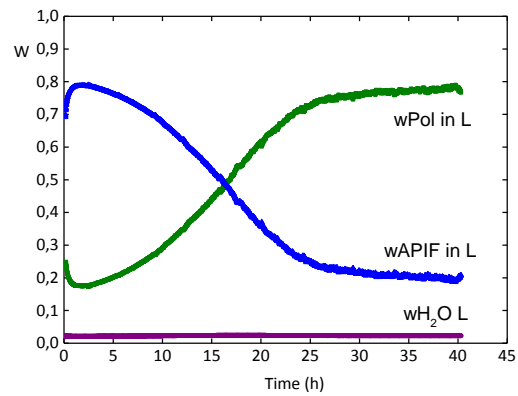


Figure 54. Concentration of components in the liquid phase for sample $w_{NIF} 0.80$, 40°C , $75\%RH$ by melting-cooling

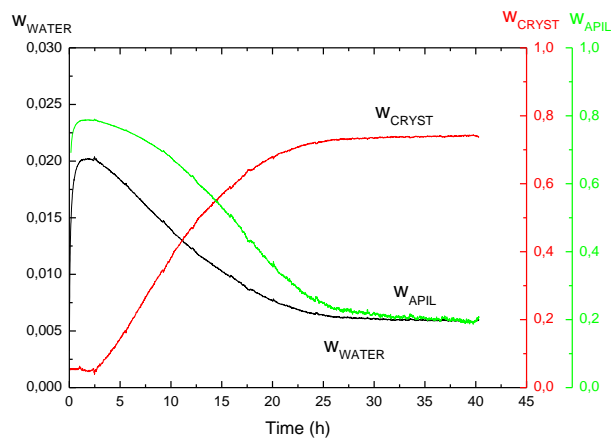


Figure 55. Evolution of concentration of crystals, water and API for sample $w_{NIF} 0.80$, $40^{\circ}C$, $75\%RH$ by melting-cooling

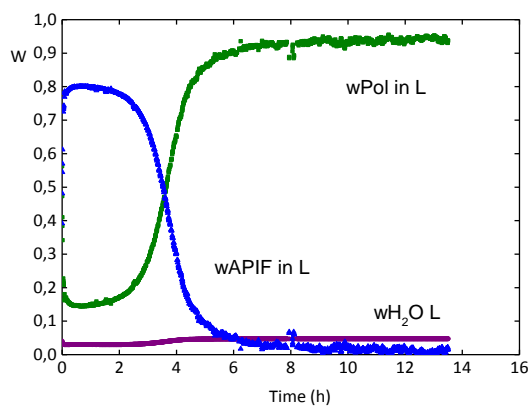


Figure 56. Concentration of components in the liquid phase for sample $w_{NIF} 0.80$, $40^{\circ}C$, $90\%RH$

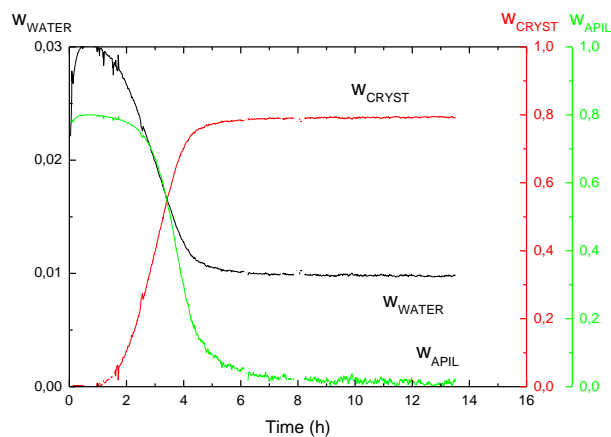


Figure 57. Evolution of concentration of crystals, water and API for sample $w_{NIF} 0.80$, $40^{\circ}C$, $90\%RH$

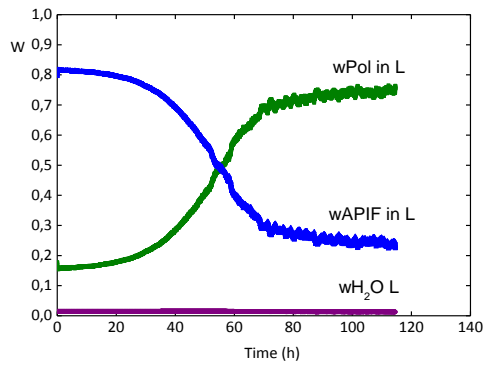


Figure 58. Concentration of components in the liquid phase for sample $w_{NIF} 0.80$, 40°C , $60\%RH$

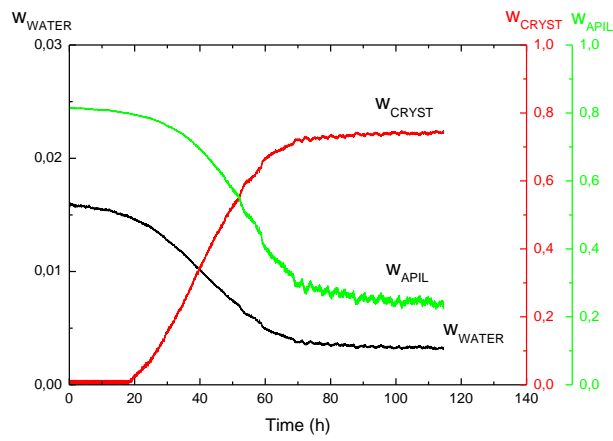


Figure 59. Evolution of concentration of crystals, water and API for sample $w_{NIF} 0.80$, 40°C , $60\%RH$

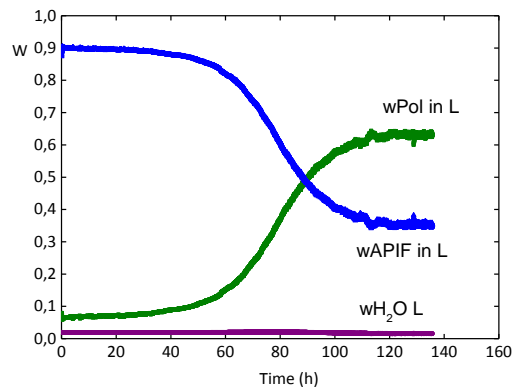


Figure 60. Concentration of components in the liquid phase for sample $w_{NIF} 0.90$, 30°C , $75\%RH$

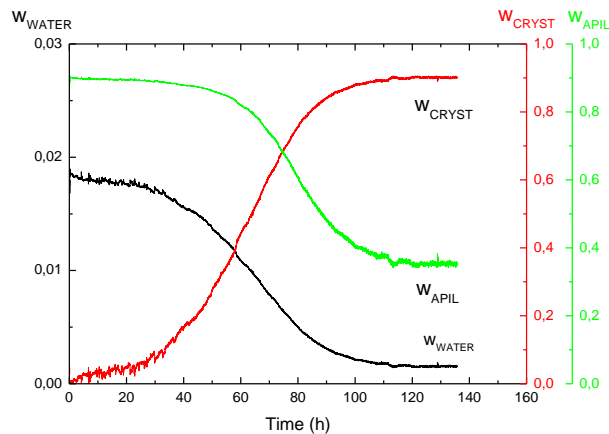


Figure 61. Evolution of concentration of crystals, water and API for sample $w_{NIF} 0.90$, 30°C , $75\%RH$

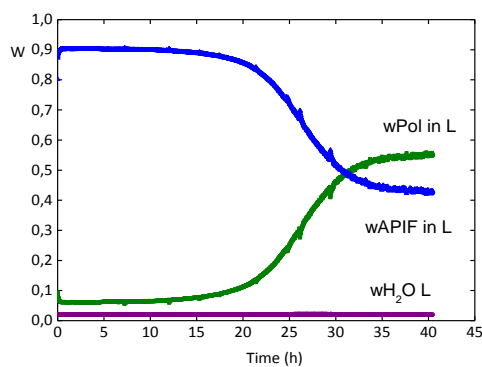


Figure 62. Concentration of components in the liquid phase for sample $w_{NIF} 0.90$, 35°C , $75\%RH$

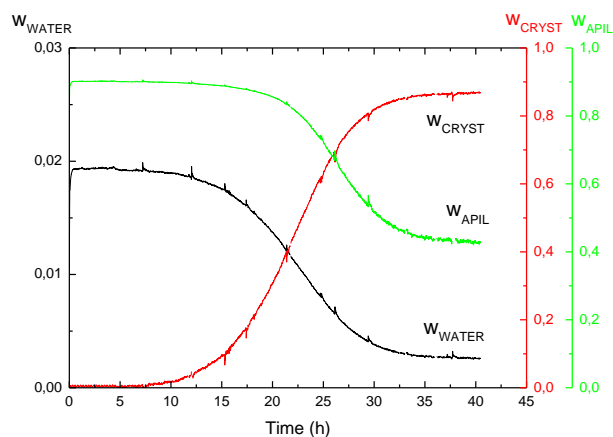


Figure 63. Evolution of concentration of crystals, water and API for sample $w_{NIF} 0.90$, 35°C , $75\%RH$

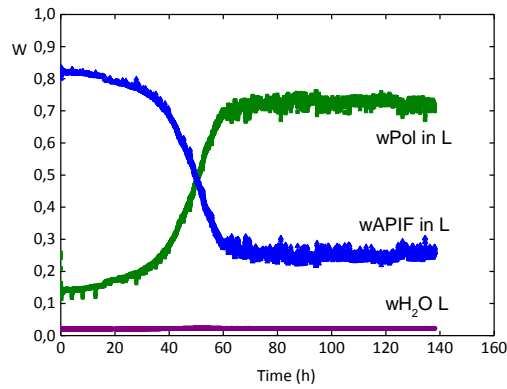


Figure 64. Concentration of components in the liquid phase for sample $w_{NIF} 0.80$, 35°C , $75\%RH$

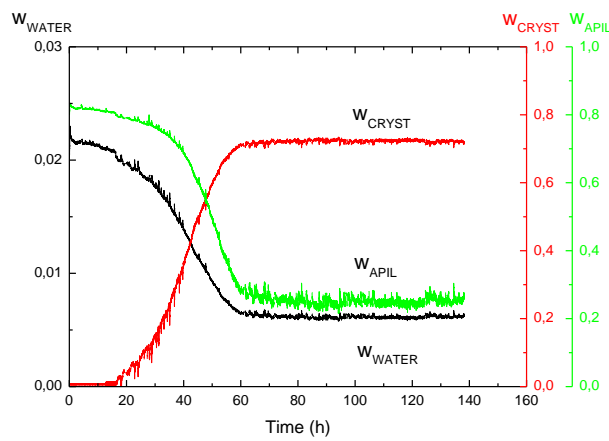


Figure 65. Evolution of concentration of crystals, water and API for sample $w_{NIF} 0.80$, 35°C , $75\%RH$

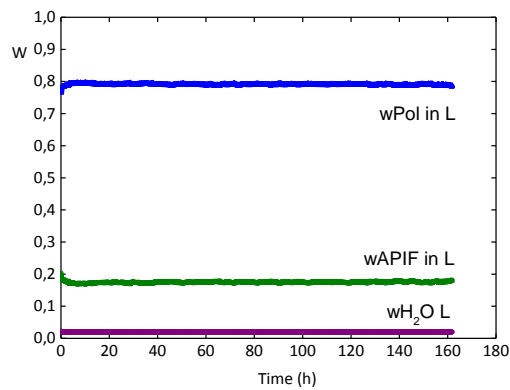


Figure 66. Concentration of components in the liquid phase for sample $w_{NIF} 0.80$, 30°C , $75\%RH$

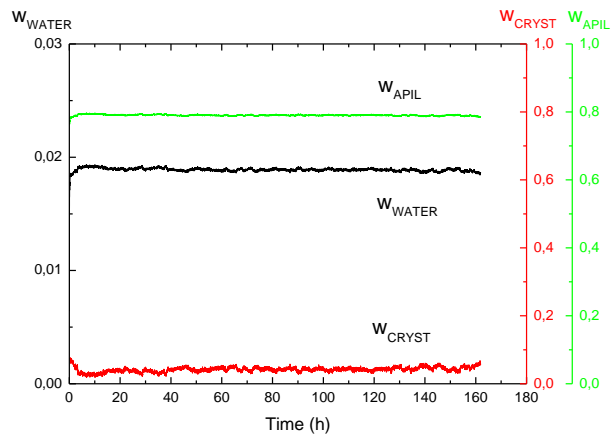


Figure 67. Evolution of concentration of crystals, water and API for sample $w_{NIF} 0.80$, 30°C , $75\%RH$

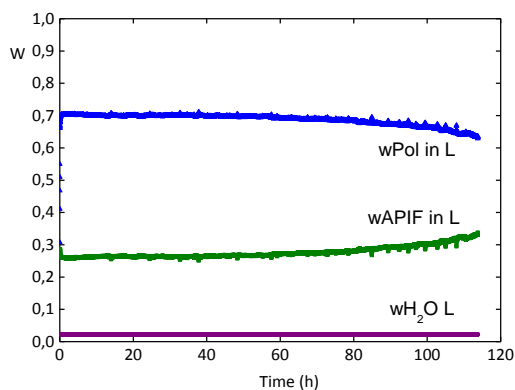


Figure 68. Concentration of components in the liquid phase for sample $w_{NIF} 0.70$, 35°C , $75\%RH$

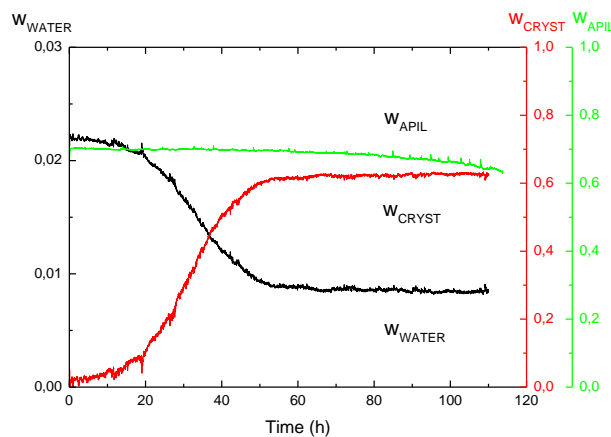


Figure 69. Evolution of concentration of crystals, water and API for sample $w_{NIF} 0.70$, 35°C , $75\%RH$

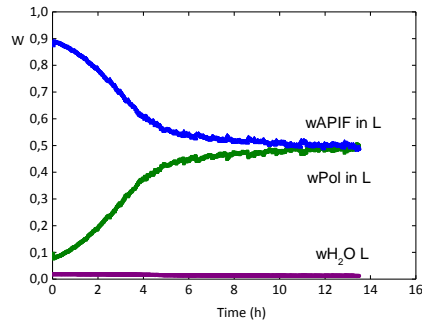


Figure 70. Concentration of components in the liquid phase for sample $w_{NIF} 0.90$ in Resomer R203s, $40^{\circ}C$, $75\%RH$

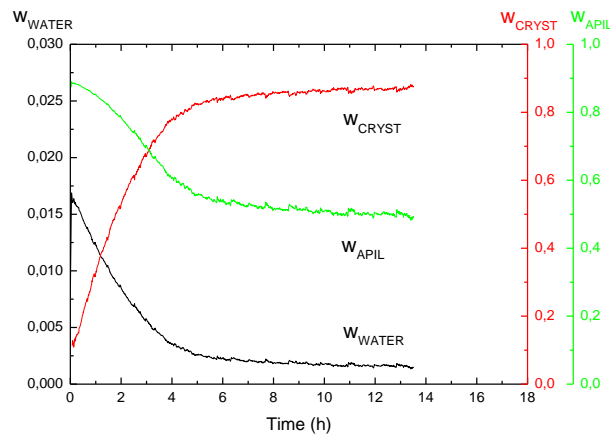


Figure 71. Evolution of concentration of crystals, water and API for sample $w_{NIF} 0.90$ in Resomer R203s, $40^{\circ}C$, $75\%RH$

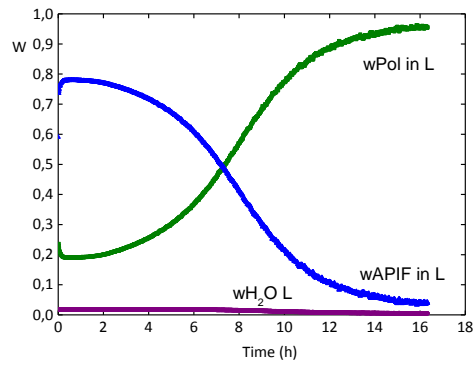


Figure 72. Concentration of components in the liquid phase for sample $w_{NIF} 0.80$ in Resomer R203s, $40^{\circ}C$, $75\%RH$

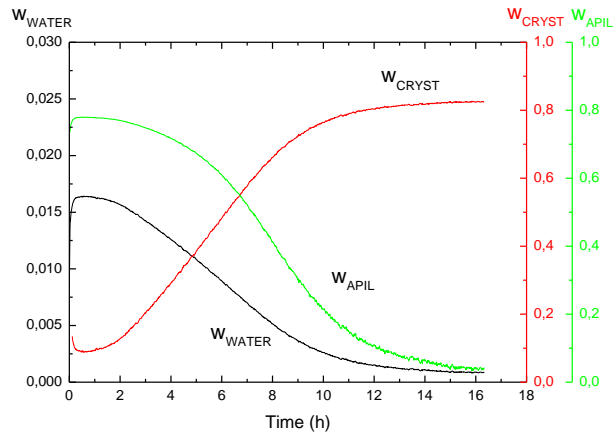


Figure 73. Evolution of concentration of crystals, water and API for sample w_{NIF} 0.80 in Resomer R203s, 40°C, 75%RH

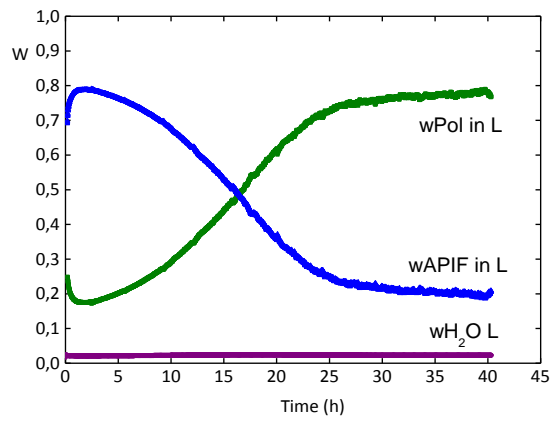


Figure 74. Concentration of components in the liquid phase for sample w_{NIF} 0.70 in Resomer R203s, 40°C, 75%RH

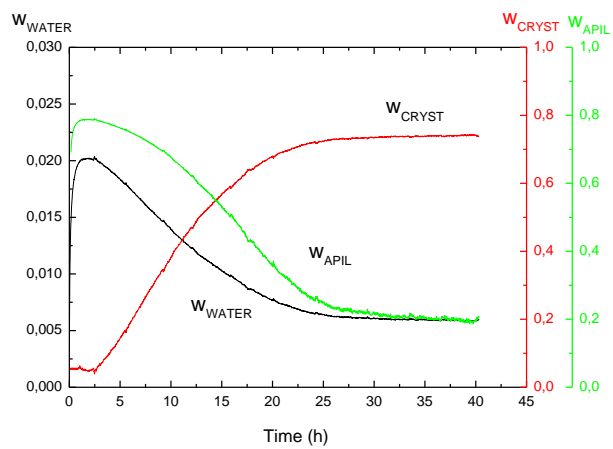


Figure 75. Evolution of concentration of crystals, water and API for sample w_{NIF} 0.70 in Resomer R203s, 40°C, 75%RH

Verification of crystallinity via PXRD and DSC

DSC measurements

Table 16. Data about samples and their DSC measurements

| Polymer | W _{NIF} (%) | Weight (mg) | T (°C) | RH (%) | Enthalpy of fusion (J/g) | Standard deviation Enthalpy of fusion (J/g) | Reverse heat flow (J/g) | Standard deviation Reverse heat flow (J/g) |
|--------------|----------------------|-------------|--------|--------|--------------------------|---|-------------------------|--|
| PVAC | 90 | 2.2 4.6 | 40 | 75 | 70.42 | 7.28 | 88.42 | 9.64 |
| PVAC | 80 | 4.4 4.4 | 40 | 75 | 65.15 | 0.30 | 72.80 | 0.40 |
| PVAC | 70 | 7.4 7.6 | 40 | 75 | 49.01 | 1.29 | 48.59 | 6.65 |
| PVAC | 90 | 6.1 8.0 | 35 | 75 | 72.88 | 0.54 | 67.11 | 21.31 |
| PVAC | 80 | 5.1 5.6 | 35 | 75 | 63.40 | 2.51 | 57.35 | 5.85 |
| PVAC | 70 | 6.0 7.5 | 35 | 75 | 46.02 | 1.70 | 40.43 | 9.75 |
| PVAC | 90 | 5.4 5.4 | 30 | 75 | 81.12 | 3.13 | 84.36 | 59.59 |
| PVAC | 80 | 7.8 7.1 | 40 | 90 | 57.49 | 1.76 | 49.62 | 19.78 |
| PVAC | 80 | 5.0 4.3 | 40 | 60 | 33.76 | 6.05 | 37.51 | 1.97 |
| PVAC350 | 80 | 5.8 4.3 | 40 | 75 | 58.23 | 2.21 | 48.01 | 17.74 |
| Resomer 203s | 90 | 7.5 7.1 | 40 | 75 | 82.38 | 2.51 | 56.41 | 25.75 |
| Resomer 203s | 80 | 8.2 7.9 | 40 | 75 | 63.95 | 1.41 | 50.67 | 1.59 |
| Resomer 203s | 70 | 6.4 6.2 | 40 | 75 | 49.33 | 4.54 | 51.89 | 7.13 |

DSC method

Table 17. DSC method

| DSC method |
|------------------------------------|
| Data storage Off |
| Equilibrate at 0.00 °C |
| Isothermal for 5.00 min |
| Data storage On |
| Modulate ± 0.796 °C every 60 s |
| Ramp 5.00 °C/min to 200.00 °C |
| Data storage Off |
| Isothermal for 5.00 min |
| Data storage On |
| Ramp 10.00 °C/min to 0.00 °C |
| Data storage Off |
| Isothermal for 5.00 min |
| Data storage On |
| Ramp 5.00 °C/min to 80.00 °C |

UV-Vis measurements

Table 18. Recorded absorbances from UV-Vis measurements

| Sample | w_{NIF} (mg) | Solution (g) | A. 1 | A. 2 | A. 3 |
|--|-----------------------------|---------------------|-------------|-------------|-------------|
| wAPI 90, 35°C, 75%RH | 5.4 | 15.197 | 2.961 | 2.958 | 2.980 |
| wAPI 90, 40°C, 75%RH | 5.4 | 12.733 | 2.872 | 2.879 | 2.877 |
| wAPI 90, Resomer R203s, 40°C, 75%RH | 5.2 | 15.418 | 2.512 | 2.799 | 2.541 |
| wAPI 90, PVAC350, 35°C, 75%RH | 5.1 | 15.104 | 2.806 | 2.807 | 2.840 |
| wAPI 85, 40°C, 75%RH | 5.2 | 15.089 | 2.295 | 2.322 | 2.330 |
| wAPI 80, 40°C, 75%RH | 5.1 | 15.137 | 2.213 | 2.212 | 2.216 |
| wAPI 80, PVAC350, 40°C, 75%RH | 5.1 | 15.171 | 2.865 | 2.874 | 2.881 |
| wAPI 80, Resomer R203s, 40°C, 75%RH | 5.2 | 15.091 | 2.338 | 2.344 | 2.352 |
| wAPI 80, Melting-Cooling, 40°C, 75%RH | 5.1 | 15.193 | 2.080 | 2.080 | 2.095 |
| wAPI 80, Melting-Cooling, 40°C, 75%RH | 5.3 | 15.442 | 2.325 | 2.302 | 2.317 |
| wAPI 80, PVAC350, 40°C, 75%RH | 5.1 | 15.087 | 2.103 | 2.105 | 2.115 |
| wAPI 80, 40°C, 75%RH | 5.1 | 15.134 | 2.182 | 2.188 | 2.192 |
| wAPI 80, 40°C, 75%RH | 5.1 | 15.121 | 2.964 | 2.978 | 2.971 |
| wAPI 80, 40°C, 60%RH | 5.6 | 15.194 | 2.792 | 2.781 | 2.799 |
| wAPI 75, 40°C, 75%RH | 5.2 | 15.108 | 2.288 | 2.293 | 2.302 |
| wAPI 70, 40°C, 75%RH | 5.2 | 15.446 | 2.805 | 2.787 | 2.818 |
| wAPI 70, 40°C, 75%RH | 5.2 | 15.355 | 2.746 | 2.651 | 2.688 |
| wAPI 70, Melting-Cooling, 40°C, 75%RH | 5.4 | 15.101 | 2.188 | 2.180 | 2.202 |
| wAPI 70, Resomer R203s, 40°C, 75%RH | 5.2 | 15.112 | 2.395 | 2.396 | 2.412 |

Calibration curve of UV-VIS Spectrophotometer

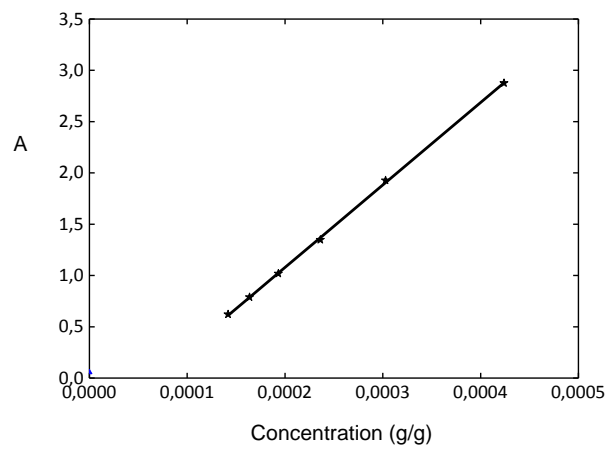


Figure 76. Calibration curve of NIF at 276 nm in acetonitrile

References

- [1] Cilurzo F., Minghetti P., Casiraghi A., Montanari L. (2002): Characterization of nifedipine solid dispersions. In: *International Journal of Pharmaceutics* 242 (2002) 313–317
- [2] Giri T.P., Kumar K., Alexander A., Ajazuddin, Badwaik H., Tripathi D.K. (2012): A novel and alternative approach to controlled release drug delivery system based on solid dispersion technique. In: *Bulletin of Faculty of Pharmacy, Cairo University* (2012) 50, 147–159
- [3] Guidance for Industry, Q7A Good Manufacturing Practice Guidance for Active Pharmaceutical Ingredients (9th April 2017). Extracted from <https://www.fda.gov/iceci/compliancemanuals/compliancepolicyguidancemanual/ucm200364.htm>
- [4] Shah S., Maddineni S., Lu J., Repka M.A (2013): Melt extrusion with poorly soluble drugs. In: *International Journal of Pharmaceutics* 453 (2013) 233– 252
- [5] Paudel A., Worku Z.A., Meeus J., Guns S., Van den Mooter G. (2013): Manufacturing of solid dispersions of poorly water soluble drugs by spray drying: Formulation and process considerations. In: *International Journal of Pharmaceutics* 453 (2013) 253– 284
- [6] Sonarome (2nd December 2014). Extracted from <http://sonarome.com/2014/12/02/spray-drying-technology/>
- [7] Particle Sciences - Technical Brief: 2011: Volume 3: Hot Melt Extrusion

[8] Chauhan A., Chauhan P. (2014): Powder XRD Technique and its Applications in Science and Technology. In: <http://dx.doi.org/10.4172/2155-9872.1000212>

[9] TA Instruments DSC Q2000 Manual

[10] Luebbert C., Sadowski G. (2016): Einfluss von relativer Luftfeuchte auf das Phasenverhalten pharmazeutischer Formulierungen. In: Thermodynamik-Kolloquium 2016, Kaiserslautern

[11] Taylor LS, Langkilde FW, Zografi G. (2001): Fourier transform Raman spectroscopic study of the interaction of water vapor with amorphous polymers. In: Journal of Pharmaceutical Sciences Volume 90, Issue 7, July 2001, Pages 888–901

[12] Baird J.A., Taylor L.S. (2012): Evaluation of amorphous solid dispersion properties using thermal analysis techniques. In: Advanced Drug Delivery Reviews 64 (2012) 396–421

[13] Gross J., Sadowski G. (2001): Perturbed-Chain SAFT: An Equation of State Based on a Perturbation Theory for Chain Molecules. In: Ind. Eng. Chem. Res. 2001, 40, 1244-1260

[14] Gross J., Sadowski G. (2002): Application of the Perturbed-Chain SAFT Equation of State to Associating Systems. In: Ind. Eng. Chem. Res. 2002, 41, 5510-5515

[15] Weinberg M.C., Birnie D.P., Shneidman V.A. (1997): Crystallization kinetics and the JMAK equation. In Journal of Non-Crystalline Solids 219 (1997) 89-99

[16] Baghel S., Cathcart H., Redington W., O'Reilly N.J. (2016): An investigation into the crystallization tendency/kinetics of amorphous active pharmaceutical ingredients: A case study with dipyridamole and cinnarizine. In: *European Journal of Pharmaceutics and Biopharmaceutics* 104 (2016) 59-71

[17] Wikipedia (7th April 2017). Extracted from https://en.wikipedia.org/wiki/Avrami_equation

[18] Zhou D., Schmitt E.A., Zhang G.G., Law D., Vyazovkin S., Wight C.A., Grant D.J.W. (2003): Crystallization Kinetics of Amorphous Nifedipine Studied by Model-Fitting and Model-Free Approaches. In *Journal of Pharmaceutical Sciences*, Vol. 92, No. 9, September 2003

[19] Caira M.R., Robbertse Y., Bergh J.J., Song M., De Villiers M.M. (2003): Structural Characterization, Physicochemical Properties, and Thermal Stability of Three Crystal Forms of Nifedipine. In: *Journal of Pharmaceutical Sciences*, Vol. 92, 2519–2533

[20] Vippagunta S.R., Maul K.A., Tallavajhala S., Grant D.J.W. (2002): Solid-state characterization of nifedipine solid dispersions. In: *International Journal of Pharmaceutics* 236 (2002) 111–123

[21] Bortolotti M., Lonardelli I., Pepponi G. (2011): Determination of the crystal structure of nifedipine form C by synchrotron powder diffraction. In: *Acta Crystallographica Section B Structural Science* ISSN 0108-7681

[22] Grooff D., De Villiers M.M., Liebenberg W. (2007): Thermal methods for evaluating polymorphic transitions in nifedipine. In: *Thermochimica Acta* 454 (2007) 33–42

[23] Gunn E., Guzei I.A., Cai T., Yu L. (2012): Polymorphism of Nifedipine: Crystal Structure and Reversible Transition of the Metastable β Polymorph. In: *Cryst. Growth Des.* 2012, 12, 2037-2043

[24] Keymolen B., Ford J.L., Powell M.W., Rajabi-Siahboomi A.R. (2003): Investigation of the polymorphic transformations from glassy nifedipine. In: *Thermochimica Acta* 397 (2003) 103–117

[25] Marsac P.J, Konno H., Rumondor A.C.F., Taylor L.S. (2008): Recrystallization of Nifedipine and Felodipine from Amorphous Molecular Level Solid Dispersions Containing Poly(vinylpyrrolidone) and Sorbed Water. In: *Pharmaceutical Research*, Vol. 25, No. 3, March 2008

[26] Prudic A., Ji Y., Luebbert C., Sadowski G. (2015): Influence of humidity on the phase behavior of API/polymer formulations. In: *European Journal of Pharmaceutics and Biopharmaceutics* 94 (2015) 352–362

[27] Lee E.H. (2014): A practical guide to pharmaceutical polymorph screening & selection. In: *Asian journal of pharmaceutical sciences* 9 (2014) 163 e175

[28] Caron V., Bhugra C., Pikal M.J. (2010): Prediction of Onset of Crystallization in Amorphous Pharmaceutical Systems: Phenobarbital, Nifedipine/PVP, and Phenobarbital/PVP. In: DOI 10.1002/jps.22232

[29] Klimakow M., Rademann K., Emmerling F. (2010): Toward Novel Pseudo-Polymorphs of Nifedipine: Elucidation of a Slow Crystallization Process. In: *Crystal Growth & Design*, Vol. 10, No. 6, 2010

[30] Marsac P.J., Konno H., Taylor L.S. (2016): A Comparison of the Physical Stability of Amorphous Felodipine and Nifedipine Systems. In: *Pharmaceutical Research*, Vol. 23, No. 10, October 2006.

[31] Konno H., Taylor L.S. (2008): Ability of Different Polymers to Inhibit the Crystallization of Amorphous Felodipine in the Presence of Moisture. In: *Pharmaceutical Research*, Vol. 25, No. 4, April 2008.

[32] Alonzo D.E., Zhang G.G.Z., Zhou D., Gao Y., Taylor L.S. (2010): Understanding the Behavior of Amorphous Pharmaceutical Systems during Dissolution. In: *Pharmaceutical Research*, Vol. 27, No. 4, April 2010

[33] Miyazaki T., Yoshioka S., Aso Y., Kawanishi T. (2007): Crystallization rate of amorphous nifedipine analogues unrelated to the glass transition temperature. In: *International Journal of Pharmaceutics* 336 (2007) 191–195

[34] Baird J.A., Taylor L.S. (2012): Evaluation of amorphous solid dispersion properties using thermal analysis techniques. In: *Advanced Drug Delivery Reviews* 64 (2012) 396–421

[35] Rumondor A.C.F., Taylor L.S. (2010): Effect of Polymer Hygroscopicity on the Phase Behavior of Amorphous Solid Dispersions in the Presence of Moisture. In: *Molecular Pharmaceutics*, 2010, 7 (2), pp 477–490

[36] Baghel S., Cathcart H., Redington W., O'Reilly N.J. (2016): An investigation into the crystallization tendency/kinetics of amorphous active pharmaceutical ingredients: A case study with dipyridamole and cinnarizine. In: *European Journal of Pharmaceutics and Biopharmaceutics* 104 (2016) 59-71